Aus der Klinik für Nephrologie und internistische Intensivmedizin
der Medizinischen Fakultät Charité – Universitätsmedizin Berlin

DISSERTATION

Senescence Signaling Pathway in the Process of Vascular Cal-
cification both in vitro and ex vivo

Seneszenz-Signalweg im Prozess der Gefäßverkalkung sowohl in
vitro als auch ex vivo

zur Erlangung des akademischen Grades
Doctor medicinae (Dr. med.)

vorgelegt der Medizinischen Fakultät
Charité – Universitätsmedizin Berlin

von

Mengdi Xia
Aus Zigong, Sichuan, China

Datum der Promotion: 03.03.2023

Preface

Parts of the results from this thesis has been published:

- Herrmann J, Gummi MR, **Xia M**, van der Giet M, Tölle M, Schuchardt M. Vascular Calcification in Rodent Models-Keeping Track with an Extented Method Assortment. Biology (Basel). 2021,10:459. (DOI:10.3390/biology10060459).

- Herrmann J, **Xia M**, Gummi MR, Greco A, van der Giet M, Tölle M, Schuchardt M. Stressor-induced "Inflammaging" of vascular smooth muscle cells via Nlrp3-mediated pro-inflammatoryauto-loop. Front Cardiovasc Med. 2021;8(1932):752305. (DOI: 10.3389/fcvm.2021.752305).

Table of Contents

List of Tables

List of figures

List of Abbreviations

Abbreviation	Meaning
ABI	Ankle brachial index
ALP	Tissue non-specific alkaline phosphatase
Bmp-2	Bone morphogenetic protein 2
Cbfa1	Core-binding factor alpha 1
CKD	Chronic kidney disease
Ctrl	Control
Cu	Copper
DAMP	Damage-associated molecular patterns
DAPI	6-diamidino-2-phenylindole
DDR	DNA damage response
DMEM	Dulbecco's modified Eagle's medium
DOX	Doxorubicin
DXA	Dual-energy X-ray absorptiometry
EBCT	Electron beam computed tomography
EC	Endothelial cells
ECM	Extracellular matrix
FBS	Fetal bovine serum
FISH	Fluorescence in situ hybridization
GAPDH	3-phosphoglycerate dehydrogenase
High-Pi	High phosphate
HKPs	Housekeeping proteins
IAC	Intimal arterial calcification
IL	Interleukin
IPA	Isolated-perfused aorta
IVUS	Ultrasound, intravascular ultrasound
MAC	Medial calcification
MiDAS	Dysfunction-associated senescence
MRI	Magnetic resonance imaging
MSCs	Marrow mesenchymal stem cells
MSCT	Multislice computed tomography

NF-κB	Nuclear factor kappa-light-chain-enhancer of activated B cells
NLRP3)	NLR family pyrin domain containing 3
OCT	Optical coherence tomography
PBS	Phosphate-buffered saline
PCNA	Proliferating cell nuclear antigen
PMSF	Phenylmethylsulfonyl fluoride
PP	Pulse pressure
PWV	Pulse wave velocity
Runx2	Runt-related transcription factor 2
SASP	Senescence-associated secretory phenotype
SA-ß-Gal	Senescence-associated β-galactosidase"
SDS-PAGE	Sodium dodecyl sulphate-polyacrylamide gel electrophoresis
siRNA	Small interfering RNA
TBST	Tris-buffered saline -Tween
TGF-β	Transforming growth factor β
TGS	Tris-Glycine-SDS
TNAP	Tissue-nonspecific alkaline phosphatase
TNF-α	Tumor necrosis factor-α
VC	Vascular calcification
VSMCs	Vascular smooth muscle cells

Abstract

Vascular calcification (VC) is an independent predictor of cardiovascular events and is associated with significant morbidity and mortality. The increased risk of these associations in chronic kidney disease (CKD) patients is more powerful. Current diagnostic and therapeutic approaches to VC are relatively limited and we need better insight into the underlying pathological mechanisms of VC as well as more effective intervention strategies. Previous studies have shown that cellular senescence is involved in VC and can promote the osteogenic transformation of vascular smooth muscle cells (VSMCs).

Therefore, the first part of this study was to establish a proper multiplex Western blot protocol for subsequent analysis of the signaling pathway in later experiments. The second and third parts of this study were designed to investigate the effect of the cellular senescence signaling pathway (p21) on vascular calcification in vitro and ex vivo. DOX induced senescence in VSMCs and activated the p21 senescence pathway while stimulating the expression of bone-associated molecules, with similar results obtained in ex vivo tissues stimulated by high phosphate. This study provides further hints for the p21-involved senescence pathway in vascular calcification in vitro and ex vivo and that it is accompanied by increased expression of multiple bone-associated molecules.

Zusammenfassung

Die Gefäßverkalkung (VC) ist ein unabhängiger Prädiktor für kardiovaskuläre Ereignisse und wird mit erheblicher Morbidität und Mortalität in Verbindung gebracht. Das erhöhte Risiko dieser Assoziationen bei Patienten mit chronischer Nierenerkrankung (CKD) ist noch stärker ausgeprägt. Die derzeitigen diagnostischen und therapeutischen Ansätze für VC sind relativ begrenzt. Deswegen brauchen wir einen besseren Einblick in die zugrunde liegenden pathologischen Mechanismen von VC und wirksamere Interventionsstrategien. Frühe Studien haben gezeigt, dass zelluläre Seneszenz an VC beteiligt ist und die osteogene Transformation von vaskulären glatten Muskelzellen (VSMCs) fördern kann.

Daher bestand der erste Teil dieser Studie darin, ein geeignetes Multiplex-Westernblot-Protokoll zu erstellen, um im weiteren Verlauf die Signalkaskade und insbesondere die Proteinexpression weiter zu untersuchen. Im zweiten und dritten Teil dieser Studie sollte die Wirkung des zellulären Seneszenz-Signalwegs (p21) auf die Gefäßverkalkung in vitro und ex vivo untersucht werden. DOX induzierte Seneszenz in VSMCs und aktivierte den p21-Seneszenz-Signalweg bei gleichzeitiger Stimulierung der Expression von knochenassoziierten Molekülen, wobei ähnliche Ergebnisse in ex vivo Geweben erzielt wurden, die durch hohen Phosphatgehalt stimuliert wurden. Diese Studie liefert weitere Hinweise dafür, dass der p21-Seneszenz-Stoffwechselweg in vivo und in vitro an der Gefäßverkalkung beteiligt ist und mit einer erhöhten Expression mehrerer knochenassoziierter Moleküle einhergeht.

1 Introduction

1.1 Vascular calcification

Vascular calcification (VC) refers to a sophisticated process causing calcium phosphate complexes to be pathologically accumulated within the vasculature, which can occur in the vessel wall's intimal layer and medial smooth muscle layer (1, 2). As a highly prevalent vascular patch phenotype, VC is regarded as part of the manifestation of the aging process and is related to atherosclerotic heart disease, hypertension, chronic kidney disease (CKD) as well as diabetes mellitus (3).

1.2 Clinical impact

VC is an independent predictor of cardiovascular events and is associated with significant morbidity and mortality (4, 5). The above-mentioned patients with VC usually suffer from inflammation and oxidative stress on a cellular level, which causes a greater pathological burden of the disease and increases adverse clinical outcomes. From a clinical perspective, patients with VC are at higher risks of adverse cardiovascular events (6, 7). The above-mentioned associations can directly elevate the risk of numerous clinical complications of VC (e.g., worsening atherosclerosis) and increase the risk of vascular events (e.g., myocardial infarction, stroke and vascular occlusion events) (8-10). In a mean of 10.1 years follow-up meta-analysis study that recruited 218,080 patients from 30 studies, the odds ratio for cardiovascular mortality from calcification individuals versus the presence of non-calcified ones was calculated as 3.94 (11). As revealed by another cohort research, which included 9,715 adults followed up for 15 years, all-cause mortality was 3% in patients without coronary artery calcification, as compared with 28% in individuals with high levels of coronary artery calcification (12). Thus, the presence of VC can be a vital surrogate marker for patient-centered outcomes as well.

1.3 Diagnostic therapy

On the whole, medial arterial calcification (MAC) is more specific in patients with CKD, probably being related to calcium phosphate exposure and abnormal bone and mineral metabolism due to decreased renal function and the years of dialysis (13, 14). In clinical practice, direct prediction of VC is not easy, and VC is primarily measured with

characteristic functional measures and diverse imaging methods. Since MAC primarily causes increased arterial stiffness, this is considered as an available proxy for the presence of vascular calcification (15, 16). Vascular stiffness is measured by pulse wave velocity (PWV), pulse pressure (PP) and ankle brachial index (ABI) (17). ABI, capable of indicating peripheral arterial disease, can indirectly measure arterial stiffness as well. Low ABI shows a relationship to vascular calcification and atherosclerosis within major arteries, whereas high ABI is related to medial calcification in peripheral and distal arteries as a sign of peripheral artery disease (18, 19). ABI was considered the preferred setting in clinical practice previously, whereas the consistency of ABI in evaluating MAC has been questioned (5). In addition, several imaging methods have been used to evaluate VC (e.g., optical coherence tomography (OCT) (17), intravascular ultrasound (IVUS), ultrasound, magnetic resonance imaging (MRI), electron beam computed tomography (EBCT), multislice computed tomography (MSCT), dual-energy X-ray absorptiometry (DXA), conventional radiography, as well as breast imaging (20)). Of the above-mentioned methods, IVUS or OCT is capable of more effectively distinguishing between MAC and intimal arterial calcification (IAC). However, since they are invasive, both of the methods are only applied when clinically indicated for selected patients (5).

For years, drugs targeting intermediates of bone and mineral metabolisms (e.g., vitamin K, phosphate-binding agents, and myo-inositol hexaphosphate) have been used to delay and slow VC progress in CKD (21-23). However, none of the evidence has been sufficient (21, 24). Thus, gaining more insights into the pathological mechanisms of VC and intervening in VC at an early stage, or even hindering its progression, may be a more effective strategy for VC treatment.

1.4 Pathophysiological mechanisms

At the tissue level, the pathogenesis of VC has been found as an active, complex, and chronic process (25, 26), which is attributed to the extracellular matrix fragmentation and disordering, endogenous inhibitor loss, senescence, or a breakdown in cellular homeostasis, and which occurs as a reaction to trauma, apoptosis, or the resolution of inflammatory and infectious insults. Moreover, this active event affects the cell-regulated process of mineralization, which is consistent with the bone formation process (10, 27, 28).

In accordance with the location and occurrence, VC has fallen into two major types (29). A type occurs in the internal layers and is related to atherosclerotic plaques, the result of lipid accumulation. Intimal calcification is related to macrophage invasion, smooth muscle cell proliferation, and extracellular matrix protein malfunction, in response to chronic artery inflammation (30). Obstructive vascular disease is attributed to unstable and rupturable plaques that grow on the inner blood artery wall. As lesions are progressing, the formation of lamellar bone and the induction of osteoblast turn out to be progressively significant (31, 32). Another type is Mönckeberg's sclerosis, i.e., medial calcification as described above, where amorphous mineral can be formed in a circumferential manner following, or in one or more of the medial layer's elastic lamellae. This type has higher prevalence among individuals with advanced aging, diabetes mellitus and CKD (33-35)

1.4.1 Vascular Calcification in CKD

In CKD, internal and medial calcification can be observed (18, 36), with medial calcification being more prevalent (37). The process is induced by a combination of pathological factors, in which high phosphate levels are considered as the critical determinants of VC in CKD (38), and phosphate has been generally considered a significant direct inducer. (39). Two distinct pathways have been postulated for the gaining of more insights into the correlation between calcium and phosphate problems and VC: a passive mechanism involving calcium phosphate precipitation in the vasculature and an active process involving vascular smooth muscle cells (VSMCs), both of which are of high importance. VSMCs can be activated from a static, differentiated condition to an active synthetic and proliferative phenotype after in vitro stimulation (40), and phosphorus triggers the osteochondral/chondrogenic phenotypic transformation of VSMCs by regulating multiple signaling pathways. As revealed by in vitro studies, VSMCs also interact closely with the formation of apoptotic vesicles in phosphate-induced phenotype transformation, and the above-mentioned cells can secrete matrix vesicles, which also increase the risk of apoptosis in surrounding cells through vesicle release (41), and that autophagy is involved (42). However, the correlation between apoptosis and autophagy remains controversial (43), and although inhibition of autophagy decreased phosphate-induced apoptosis in VSMCs, it may not have been achieved by reducing apoptosis in VSMCs, but rather by lowering matrix vesicle release (25, 44). Thus, the process of phosphate-induced VC is controlled by an extremely complex network of cellular signaling pathways characterized by

numerous crosstalk and close interactions between the above-mentioned signaling cascades (45, 46).

1.4.2 Cellular senescence in VC

According to its definition, cellular senescence refers to the ineffective repair of DNA damage and causes irreversible growth arrest (47). Due to eukaryotic cells' usual inability to maintain telomere length, telomere is progressively shortened with the respective division, the DNA damage response (DDR) is activated, and this causes replicative senescence to not diminish over time. This pathway binds to the cell cycle protein-dependent kinase inhibitor p21, and the tumor suppressor gene p53, which is then stabilized through the retinoblastoma protein hypophosphorylation and p16 activation, leading to proliferation-promoting genes being silenced (48-50). VSMCs senescence complies with typical features of senescent cells. During VC, senescent VSMCs located in the media of the vessel affect the development of VC by introducing the p53/p21 classical senescence pathway (51), which plays an essential role in medial calcification pathophysiology through increased osteoclast transition and upregulation of tissue-nonspecific alkaline phosphatase (TNAP), core-binding factor alpha 1 (Cbfa1), and type I collagen (52). There is decreased expression of Cbfa1 and reduced calcification after knockdown of p21 siRNA in VSMCs (53). In addition, senescent cells acquire extensive morphological and functional changes, expressing lysosomal activity-associated senescence-associated β-galactosidase (SA-ß-Gal) and phospho-histone H2A.X. Another prominent characteristic of senescent cells refers to senescence-associated secretory phenotype (SASP) development (54, 55). The high phosphorus and calcium status of CKD patients can further increase SASP levels, and up-regulated SASP inflammatory markers are related to promoting osteogenic differentiation and calcification in VSMCs (56). At the same time, activation of SASP acts as a driver of IL-6 and MCP1 secretion, which in turn promotes calcification (54, 57).

1.4.3 p21 in Senescence Pathway

It is well known that p21 is a cell cycle inhibitor that has a physical interaction with cyclin-CDK4/6, -CDK1 and -CDK2 complexes' activity for blocking the progression of the cell cycle in the transition of G1/S and G2/M. Controlling E2F activity can mediate the cell growth regulation using p21 (58-60). CDK and regulatory component cell cycle proteins regulate cell cycle progression in mammals, and cell cycle progression is activated by

Rb's partial phosphorylation by CDK-cell cycle proteins, whereas p21 can disrupt the above-mentioned relationship and prevent the progression of the cell cycle (61, 62). For the p21 gene, it has been initially found that wild-type p53 protein can induce this gene (63). Cell cycle arrest within the G1/S phase refers to a p53-dependent mechanism controlled by paclitaxel, transforming growth factor β (TGF-β), and oncogenic Ras. It is possible that it is linked to the cycle E and cyclin A/CDK genes (64-66). Besides growth arrest, p21 can also mediate cellular senescence through p53-dependent pathways, and the overexpression of p21 was initially discovered in normal human diploid senescent cells (67). As indicated by existing studies, p21 is capable of mediating senescence through a ROS-based mechanism that does not require the binding of proliferating cell nuclear antigen (PCNA) or CDK inhibition (68), and that p21 increases intracellular ROS levels in p53-negative cancer cells and normal fibroblasts (69).

1.5 Vascular Calcification Models

As mentioned above, VC is a complex process that involves complex interactions between many different cell types and mechanistic signals (70, 71). It is because the development of VC may be impacted by multiple factors and the underlying mechanisms of VC are not fully revealed that various research models have emerged, which can fall into in vitro, ex vivo as well as in vivo models.

In vitro model reduces the interferences from different cell types and complex interacting factors, so insights can be more easily gained into the multiple mechanisms resulting in VC (70). A variety of cell types that make up the vascular system, including the external, media, intima and circulating, may serve as vehicles for models of VC (72-76). Among them, the crucial point of VC should be the cellular transformation of VSMCs to osteoblast-like cells (77, 78). Thus, different sources, including human, rat and mouse VSMCs are currently the most extensively used in vitro model to investigate medial VC (74, 75, 77).

The fact that this animal model is analyzed for the whole organism reflects the physiological context, allows for monitoring the progression of calcification in a reasonable time, and that a longitudinal study method with the use of the identical animals as controls is capable of reducing statistical differences and decreasing the required sample size, the above-mentioned points fully demonstrate the advantages of in vivo models for

calcification studies. Additionally, ex vivo models may provide a valuable alternative. This direct placement of vessels in calcification media allows for elementary and easy experimental procedures and for taking less time to accurately assess vascular calcification while maintaining the entire structure of the vessel (79, 80).

1.6   Aims of the study

Existing studies have shown that cellular senescence is involved in the process of VC, which can facilitate the osteogenic transformation of VSMCs. Besides, phosphate may induce ROS production and oxidative stress in VSMCs, exacerbating cellular senescence and further facilitating cellular phenotypic transformation. It is a process in which the classical pathway of p21 cellular senescence may be involved. The high phosphate state, playing a critical role in causing VC in CKD patients, is mainly prone to occur after impaired renal function, which leads to an elevated risk of death as well as cardiovascular events.

Accordingly, this paper aimed to:

1) Establish an optimized multiplex Western blot protocol that could be exploited to quantify cellular and vascular proteins, and especially to study senescence and osteogenic transformation;

2) Further explore the impact exerted by the cellular senescence signaling pathway (p21) on VC in the VSMCs stimulated; and

3) Validate the modeling of the high phosphate medium in ex vivo and verify the expression of p21 and bone-related molecules' protein level in the tissue.

2   Methods

2.1   Manufacturer information on reagents, devices and software

Table 1: Materials for cell culture and ex vivo

Medium and materials for cell culture	Manufacturer
Dulbecco's modified Eagle's medium (DMEM)	Biochrom AG, Berlin, Germany
Fetal bovine serum (FBS)	Biochrom AG, Berlin, Germany
Penicillin/streptomycin	Biochrom AG, Berlin, Germany
Phosphate-buffered saline (PBS)	Biochrom AG, Berlin, Germany
NaH_2PO_4	Merck KGaA, Darmstadt, Germany
Vitamin C	Sigma Aldrich, Missouri, USA
DOX	Thermo Fisher Scientific, Massachusetts, USA

Table 2: Materials for Western Blot

	Materials	Manufacturer
Electrophoresis	Mini-protean® TGX™ Precast Gels, 12%, 10-well comb, 50ul/well.	Bio-Rad, California, USA
	Mini-protean® TGX™ Precast Gels, 4-20%, 10-well comb, 50ul/well.	Bio-Rad, California, USA
	Mini-protean® TGX™ Precast Gels, 4-20%, 10-well comb, 30ul/well.	Bio-Rad, California, USA
Transfer	Trans-Blot Turbo, Mini Format, 0.2µm PVDF, Single Application.	Bio-Rad, California, USA
	Trans-Blot Turbo, Mini Format, 0.2µm Nitrocellulose, Single Application.	Bio-Rad, California, USA
	Trans-Blot Turbo RTA Mini 0.2 µm PVDF Transfer Kit.	Bio-Rad, California, USA
Detection	Clarity and Clarity Max ECL Western Blotting Substrates.	Bio-Rad, California, USA

Table 3: Antibodies

Antibodies		Manufacturer
Primary Antibodies	Rabbit-anti-β-Actin	Santa Cruz Biotechnology, California, USA
	Mouse- anti-β-Actin	Cell Signaling Technology, Massachusetts, USA
	Mouse-anti-GAPDH	Cell Signaling Technology, Massachusetts, USA
	Rabbit-anti-Bmp-2	Abcam, Cambridge, UK
	Rabbit-anti-p21	Abcam, Cambridge, UK
	Rabbit-anti-ALP	Invitrogen, Massachusetts, USA
	Rabbit-anti-Runx2	Santa Cruz, Texas, USA
Secondary Antibodies	IgG-goat anti-rabbit-StarBright Blue700	Bio-Rad, California, USA
	IgG-goat anti-mouse-StarBright Blue700	Bio-Rad, California, USA
	IgG-goat anti- mouse-StarBright Blue520	Bio-Rad, California, USA
	goat anti-rabbit-Alexa Fluor 555 IgG	Bio-Rad, California, USA
	IgG- rabbit anti-goat	Bio-Rad, California, USA

Table 4: Reagents for qRT-PCR

	Reagents	Manufacturer
mRNA isolation	RLT Buffer	QIAGEN, Venlo, Netherlands
	ß-mercaptoethanol	QIAGEN, Venlo, Netherlands
	RNeasy Kit	QIAGEN, Venlo, Netherlands
cDNA synthesis	RT-Buffer	Thermo Fisher Scientific, USA
	dNTP's	Thermo Fisher Scientific, USA
	Random Primer	Thermo Fisher Scientific, USA
	MultiScribe RT	Bio-Rad, CA, USA
PCR	iQ SYBR Green Supermix	Bio-Rad, CA, USA
	Primers	TIB Molbiol, Berlin, Germany

Table 5: Primers for PCR

Gene	Fwd 5´-3´ Rev 5´-3´	Manufacturer
β-Actin	TCG CTG ACA GGA TGC AGA AG CTC AGG AGC AAT GAT CTT GAT	Tib Mol, Berlin, Germany
p21	TAT GTA CCA GCC ACA GGC AC ATC GGC GCT TGG AGT GAT AG	Tib Mol, Berlin, Germany
Cbfa1	GCC GGG AAT GAT GAG AAC TA GGA CCG TCC ACT GTC ACT TT	Tib Mol, Berlin, Germany
ALP	TCC GTG GGT CGG ATT CCT GCC GGC CCA AGA GAG AAA	Tib Mol, Berlin, Germany

Table 6: Other reagents

Reagents	Manufacturer
Invitrogen™ NP40 Cell Lysis Buffer	Thermo Fisher Scientific, Massachusetts, USA
RIPA Lysis and Extraction Buffer	Thermo Fisher Scientific, Massachusetts, USA
Colorimetric Calcium Assay Kit	Sciencell Research Laboratories, Faraday, USA
Pierce™ BCA Protein Assay	Thermo Fisher Scientific, Massachusetts, USA
Roti®-Block	Carl Roth, Karlsruhe, Germany
4x Laemmli Sample Buffer	Bio-Rad, California, USA
Ponceau S Staining Solution	Sigma Aldrich, Missouri, USA
cOmplete Mini Protease inhibitor	Merck KGaA, Darmstadt, Germany
Total Protein Extraction Kit for Blood Vessels	Invent Biotechnologies, Minnesota, USA

Table 7: Materials used in Alizarin red staining

Materials	Manufacturer
Formalin	Sigma Aldrich, Missouri, USA
Alizarin Red S solution	Sigma Aldrich, Missouri, USA
Lab Tek slide	Merck KGaA, Darmstadt, Germany

Table 8: Devices and software

Devices	Manufacturer	Software	Manufacturer
Plate reader	Multiskan Spectrum	Bio-Plex Manager software 6.1	Bio-Rad, CA, USA
Axiovert 200M microscope	Zeiss, Jena, Germany	GraphPad Prism statistical software v6.0	GraphPad, CA, USA
Bio-Rad T100 and C1000 Thermal Cycler	Bio-Rad, CA, USA	ZEN 2 (blue edition) software	Zeiss, Jena, Germany
Eppendorf thermomixer 5436	Eppendorf, Hamburg, Germany	BioRad CFX Manager Software 3.1	Bio-Rad, CA, USA
QiaCube	QIAGEN, Venlo, Netherlands	Fluoroskan Ascent®	Thermo Fisher Scientific, Massachusetts, USA
Trans-Blot®Turbo™ Transfer System	Bio-Rad, CA, USA	Image Lab Software 5.2.1	Bio-Rad, CA, USA
ChemiDoc Imaging Systems	Bio-Rad, CA, USA	Image Lab touch Software	Bio-Rad, CA, USA
iEMS Reader MF	Thermo Fisher Scientific, Massachusetts, USA		

2.2 Animals

All animal experiments were performed under conditions that alleviated the suffering of animals to the greatest extent based on the EU Directive 2010/63/EU. After we intraperitoneally injected sodium pentobarbital (400 mg/kg body weight) and verified the missing reflexes, the abdominal skin of the rat was disinfected with 70% ethanol and fixed on an operating table. The rats were dissected layer by layer with sterilized instruments and the aorta (i.e., the thoracic aorta and aortic arch) was completely removed. The aorta were washed with PBS + penicillin (100 U/ml) and streptomycin (0.1 mg/ml). The outer membrane and connective tissue from the aorta were removed in the solution culture dish. Afterwards, we transferred the aorta to a novel petri dish in which streptomycin (0.1 mg/ml) solution and fresh PBS + penicillin (100 U/ml) were contained to perform the next step.

2.2.1 Isolating primary cells

For the culture of primary VSMCs, the outgrowth method was used. After removal of the adventitia, the aortas were incised longitudinally on tin foil with a small amount of culture medium (Dulbecco's Modified Eagle Medium (DMEM) covering 1 g/l glucose with 0.1 mg/ml streptomycin, 100 U/ml penicillin, as well as 15% fetal calf serum (FCS)) and gently scraped off with a sterile knife lining, taking care to keep the vascular tissue moist. Medium was pre-added (DMEM containing 1 g/l glucose with 0.1 mg/ml streptomycin, 100 U/ml penicillin, as well as 15% fetal calf serum (FCS)) to the culture flask and the aortas were cut into small pieces (approximately 4 mm^2 each), transfered to the bottom of the culture dish and unfolded. This was incubated obliquely for 5 min at 37°C in a 5% CO_2 incubator. After ensuring that we attached all tissue pieces to the flask bottom, we laid the flask flat so that all tissue pieces were immersed in the medium solution for incubation. Then we placed the flask in the incubator for 5-7 d and obtained the primary cells migrated from the medium explants. Figure 1 illustrates the flow chart.
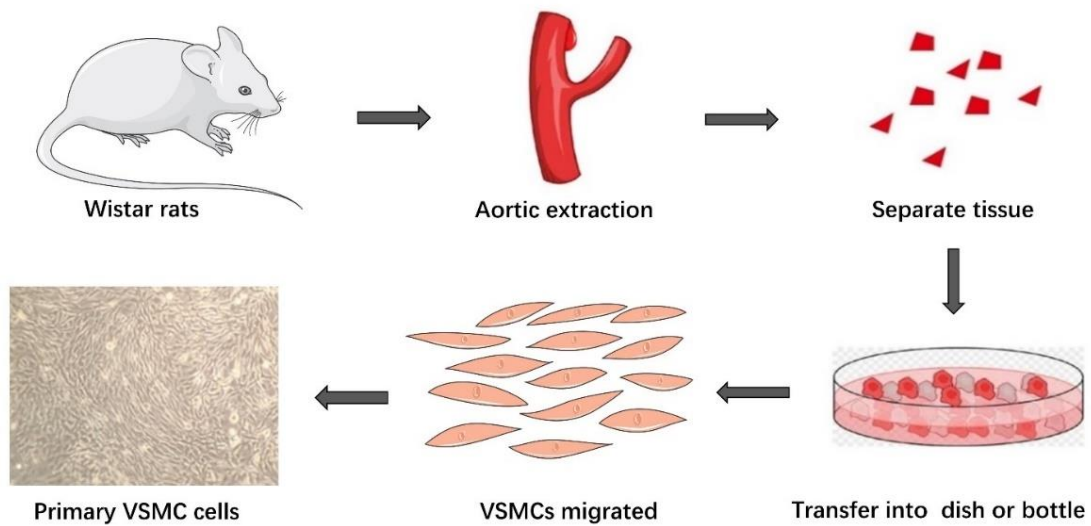
Figure 1: Flow chart of isolated primary cells. (Figure created by author using Servier Medical Art.)

2.2.2 Ex vivo preparation

For ex vivo settings, after removing the adventitia, the aortas were taken one by one from the PBS, a 10 µl pipet tip was put through the aortic ring and the rings were gently moved down along the tip for three times to remove endothelium. Subsequently, the aortas were cut with the use of a scalpel in 3-4 mm rings and placed in an 8-well plate filled with incubation media (500 µl). We placed the 8-well plate within the incubator based on a 5% humidified CO_2 atmosphere at the temperature of 37 °C. Figure 2 illustrates the flow chart.

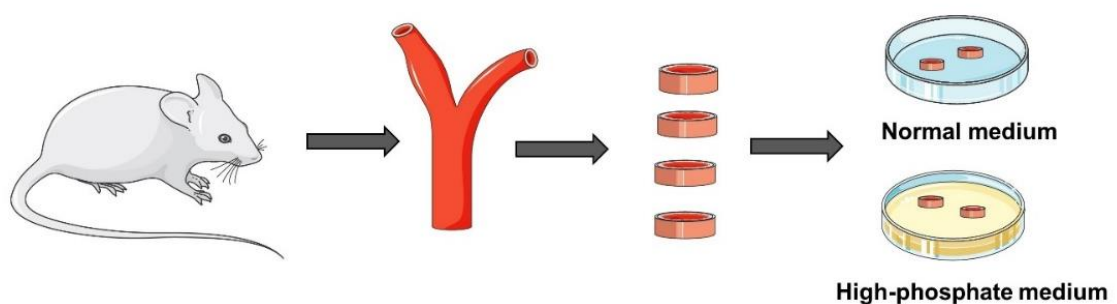**Figure 2:** Flow chart of ex vivo preparation. (Figure created by author using Servier Medical Art.)

2.3   Cell culture

We cultured VSMCs within DMEM of 1 g/l glucose containing 0.1 mg/ml streptomycin, 100 U/ml penicillin, as well as 10% fetal calf serum (FCS). We cultured the cells using a humidified incubator with 5% carbon dioxide at 37°C. 4 to 6 passages of cells were used for experiments.

2.4   Stimulation

2.4.1   Long stimulation in vitro

In the in vitro experiments, we induced the calcification by exposing cells to DMEM made up of 4.5 g/l glucose and stable glutamine, and we added 0.1 mg/ml streptomycin, 100 U/ml penicillin, 5 mmol/l inorganic phosphate, 284 mol/l ascorbic acid and 15% FCS to the mix. High-phosphate Medium (High-Pi M) or VSMCs were stimulated with 10nM DOX, 100nM DOX for 14 d in High-Pi M. We carried out the culture of the controls using DMEM of 4.5 g/l glucose and supplemented with 0.1 mg/ml streptomycin, 100 U/ml penicillin and 15% FCS (Control Medium (Ctrl M)). The cells achieved growth to confluence before induction of calcification. Calcification was assessed after stimulation for 14 days.

2.4.2   Short stimulation in vitro

VSMCs were stimulated with 500nM DOX, 1000nM DOX for 24 h, 48h and 72h.

2.4.3   Stimulation ex vivo

In ex vivo experiments, calcification was assessed 14 days by exposing the cells and aortic rings to DMEM without glutamine, with the rest of the added material being the same as the cell culture medium.

2.5   Alizarin red staining and calcium content

2.5.1   In vitro experiments

To produce 2% Alizarin Red S solution, 2 g of Alizarin Red S was dissolved in 100 mL distilled water, and the pH was adjusted to 4.1- 4.3. The cells were fixed for 10-15 min in 4% buffered formaldehyde, then rinsed in distilled deionized water and PBS. Next, the cells received a treatment using alizarin red solution (2%, pH 4.2) for 20 min before being

washing again. Lab Tek slides were embedded by embedding for each well and covered with glass. The imaging was done with a Zeiss Axiovert 200M microscope and ZEN 2 (Blue edition) software.

For quantification of calcification, VSMCs decalcified in 0.6 mol/l HCl overnight. After decalcification, cells were washed with PBS and lysed in 0.1 mol/l NaOH/0.1% SDS buffer. The protein content was quantified using BCA protein assay kit. According to the manufacturer's recommendation, calcium content was quantified using the colorimetrical o-cresolphthalein method. Protein content was used for normalization.

2.5.2 Ex vivo experiments

The aortic rings were fixed throughout the night, transported in 70% ethanol, and automatically placed in paraffin. We deparaffinized and hydrated the paraffin sections using 70% alcohol and rinsed the sections with distilled water (ddH2O). Subsequently, we stained the sections using alizarin red (pH 4) for from 30 sec to 5 min. The reaction was checked under the microscope, then the excess dye and blotted portions were shaked off. Afterward, we dehydrated the slices and then cleaned them in xylene and fixed them in a synthetic mounting medium. We conducted the imaging under a Zeiss Axiovert 200M microscope and using ZEN 2 (Blue edition) software.

Quantitative of calcification content was performed similarly to in vitro, aortic rings were decalcified in 0.6 mol/l HCl for 24 hours. After decalcification, they were washed with PBS and lysed in 0.1 mol/l NaOH/0.1% SDS buffer. Protein and calcification were quantified using the same approach as for cells. Protein content was used for normalization.

2.6 Extract Protein

2.6.1 For Cells

We washed the cells in the culture flasks using cold PBS and repeated the washing twice, with the flasks always kept on ice. The culture flasks were filled with RIPA buffer (300 µl/bottle, RIPA buffer 6.5 ml with 1/2 table protease inhibitor) and incubated on ice for 5 min. Cells were scraped from the bottom of the culture flask into Eppendorf tubes using a 300 mm spatula. Eppendorf tubes were incubated on ice for 30 min, with vortexing for 20 sec at 10 min intervals. Finally, the Eppendorf tubes were centrifuged for 20 min at

16,000 rpm, at 4℃. The supernatant was transferred into fresh tubes (this being extracted total protein).

2.6.2 For Tissue

For protein extraction from vascular tissues, we made various attempts, including with TissueRuptor, liquid nitrogen milling and an Invent kit. Due being impacted by the small tissue samples and the unique structure of vessels, the tissues were not adequately homogenized when TissueRuptor was applied. For this reason, the method above was eliminated first. The liquid nitrogen milling method and the Invent kit protocol were respectively used to extract vascular tissue proteins during the experiment.

The first method was liquid nitrogen milling, in which the artery rings were frozen and milled in a pre-frozen mill with liquid nitrogen. Subsequently, the NP40 buffer (3.5 ml aliquot NP40 + 1/2 table protease inhibitor + 0.5 mM phenylmethylsulfonyl fluoride (PMSF)) was added after sufficient milling, during which the liquid nitrogen was added after evaporation. The tissue was mixed with the lysate buffer and transferred to an Eppendorf tube, incubated on ice for 20 min, and then placed in a pre-chilled ultrasonic water bath with ice for 10 sec. Lastly, the Eppendorf tubes were centrifuged for 10 min at 12,000 rpm at 4℃. The supernatant was transferred into fresh tubes (extracted total protein).

The second method that we used to extract tissue proteins was with the Invent Kit, in which arterial rings were cut with scissors into small pieces (1x1 mm or smaller) at RT and placed in a filter cartridge with a collection tube. Protein extraction powder was introduced onto the top of the tissue pieces, and then a denaturing buffer was added. The tissue mixture was fully milled in the collection tube and incubated at RT for 10 min. Finally, the collection tubes were centrifuged for 1 min at 12,000 rpm at RT. The filter was removed and discarded. The supernatant was transferred to fresh tubes (this was the total protein extracted).

2.7 BCA assay

The BCA Protein Assay combines protein-mediated reduction of Copper $(Cu)2+$ to $Cu1+$ with colorimetric detection using a bicinchoninic acid-containing reagent. The response generally falls into the two stages below. The chelation of copper with protein in the alkaline environment generated is the first stage in the process, resulting in a light blue

complex. At the second stage, the purple color shift is attributed to two molecules of Bicinchonininc acid reacting with the reduced cation produced in step one (the reaction is presented in Figure 3). The experiment was performed in accordance with procedure, including preparing the working reagent, mixing the samples and working reagent, and incubating for 30 min at 37°C. Lastly, the plates were read at a wavelength of 560 nm. By adjusting to the standard curve, the outcome was calculated.
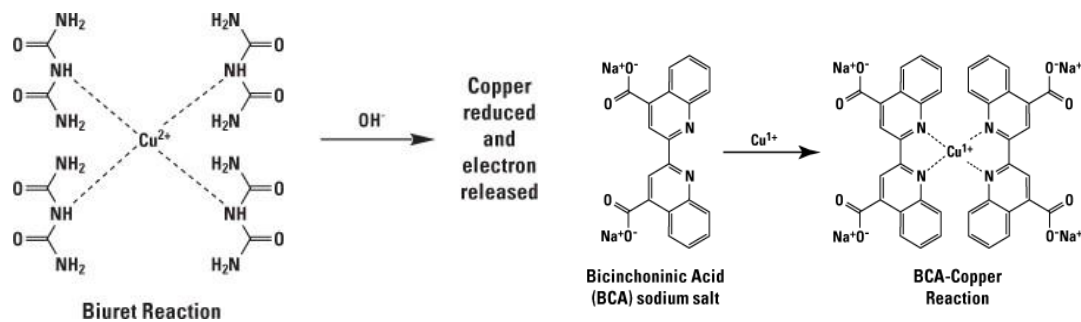

Figure 3: The response of bicinchoninic acid in the assay.

(https://thepencillog.wordpress.com/2020/01/01/the-principle-of-the-bca-assay/)

2.8 Establishment of multiplex Western Blot Protocol

We used sodium dodecyl sulfate-polyacrylamide gel electrophoresis (SDS-PAGE) to perform the Western blot assay for the separation of proteins of different molecular weight sizes. Next, we placed the proteins in a solid-phase carrier. The carrier adsorbed proteins within a non-covalent bond. The peptide under the separation using electrophoresis had intact biological activity and the kept type. We employed the protein or peptide on the solid-phase carrier as an antigen. The antigen was immunoreacted with the corresponding primary antibody and then had a reaction with enzyme or isotope-labeled secondary antibody for a specific detection through substrate development or radiolucent autoradiography (81, 82).

The conventional Western blot method requires sample preparation, gel preparation, electrophoresis, membrane transfer, blocking, as well as antibody incubation and development, for which it usually takes 2-3 days to complete the whole operation process. Using a combination of the Rapid Blotting Workflow provided by Bio-rad and the individual situation of our laboratory, we established an individualized fluorescence Western Bolt Procotol, retaining the advantages of conventional Western blot methods with more streamlined steps (e.g., electrophoresis and membrane transfer, digital fluorescence imaging technology and total protein normalization), which improved the sensitivity and

reliability of the results. The following are the major steps and equipment for the protocol established in this paper (Figure 4).

2.8.1   Preparation

The corresponding buffers required for Western blot were configured in accordance with the recipe below. We selected 1x Tris-Glycine-SDS (TGS) as the running buffer and 1x Tris-buffered saline (TBS) -Tween (T) as the washing buffer in our protocol.
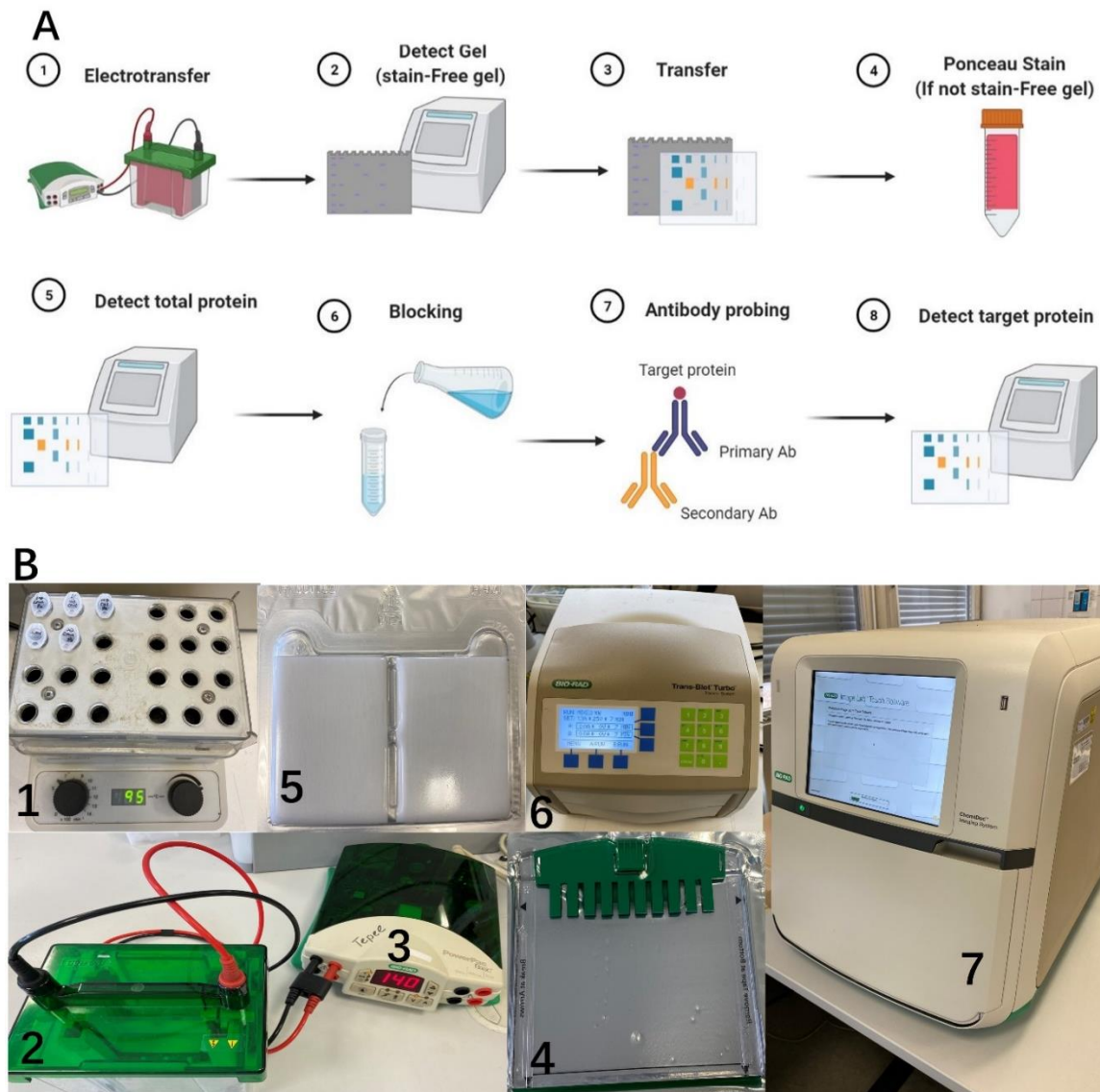

Figure 4: Diagram (A) and materials (B) in Western Blotting Procedure**:** 1. Eppendorf thermo-mixer, 2. Bio-rad electrophoresis chamber, 3. Bio-rad power supply, 4. Precast TGX gel, 5. Trans-Blot Turbo, 6. Trans-Blot® Turbo™ Transfer System, 7. ChemiDoc Imaging System. Figure 4 (A) created using BioRender by the author.

2.8.2   Electrophoresis with Gels

With Precast TGX gel, we reduced the steps of gel preparation, unified the quality of the gel, and tested the protein separation effect of 12% and 4-20% precast (or stain-free) gel. 4-20% gel was found to be suitable for separating polypeptides from 2-400kD, and 12% of the gluing could be suitable for separating polypeptides from 12-200kD. At this point, if we were using the stain-free gel, we would develop it on ChemiDoc before transfer.

2.8.3   Transfer to the membrane

We used the Trans-Blot®Turbo™ Transfer System, which significantly reduced the time taken and provided more stable results than conventional tank blotting. Since we aimed to establish a multiplex Western blot protocol, multiple antibodies needed to be incubated in one membrane. We tested PVDF and Nitrocellulose membranes in our Western blot.

2.8.4   Antibody Incubation

To establish a multiplex Western blot protocol, we attempted to incubate primary antibodies simultaneously (e.g., incubating different target proteins from host-rabbit and host-rat in one blot) and selected the secondary antibodies corresponding to each of them for incubation to fulfill our aim.

2.8.5   Imaging and Protein quantification

After transferring from stain-free gel, we used the ChemDoc MP imaging system to image the total protein amount. After the immunoblot, we used the ChemDoc MP imaging system again to image the target protein. For protein quantification, the intensity of the blotted bands was analyzed with Image Lab (version 5.2) software. Using the above-mentioned methods, we determined the p21, ALP, Cbfa1 protein and Housekeeper proteins (HKPs) contents.

2.8.6   Ponceau S staining

The membrane before blocking was immersed in sufficient ponceau S staining solution (50ml tube) and then stained for 5 min. Subsequently, the membrane was rinsed with distilled TBS-T box till the background was clear and observed.

2.9 Gene expression

The levels of p21, ALP, Cbfa1, IL-1β and IL-6 mRNA were tested through qRT-PCR. VSMCs were serum starved for 24 h in flasks before total mRNA was extracted using the Qiagen RNeasy Kit following the manufacturer's instructions. The surgery was carried out with a QiaCube or by hand. The cells were washed twice with ice-cold PBS before they were lysed in 350 µl RLT Buffer supplemented with 1%-mercaptoethanol. After each kit was introduced to the RNeasy spin column and cryopreserved at -80°C for 2 h, the mRNA was extracted by numerous short centrifugations, and then the mRNA was washed down from spin columns with 50 µl RNase-free water into collection tubes. Afterward, we used random primers to produced cDNA from mRNA. The reaction time was 10 min at 25°C and 2 h at 37°C. Lastly, using specified primers, the target and housekeeping genes were measured by PCR. Each well (384-well plate) had a 10 µl reaction volume. The PCR settings were 3 min at 95°C initial denaturation, 15 sec at 95°C denaturation for 39 cycles, primer annealing for 15 sec at 60°C, and DNA extension for 1 min at 72°C. The Bio-Rad CFX Manager Software 3.1 was used to assess the data.

2.10 Statistical analyses

We performed the experiments in at least three separate experiments to ensure that the results were repeatable. The figure legend lists the number of experiments for the respective subject. Unless otherwise stated, data were expressed as means with standard error (SE). The results for Western blot were regulated expression volumes for the validation of targets' expression. We used GraphPad Prism program 8.0 (GraphPad Software Inc, La Jolla, CA, USA) to determine statistical significance. A statistically significant p value <0.05 was adopted.

3. Results

3.1 Establishment of multiplex Western Blot and Optimization conditions

The Western blot process can fall into the stages of sample preparation, boiling, loading, electrophoresis, transfer and immunoassay. At the first stage, clear and regular bands were not obtained using conventional methods. Lastly, through conducting the trial and by exploring various factors, we finally achieved the following optimizations:

1) Boiling time: the final setting was 15 min. Most target proteins were small molecular weight proteins, less than 25 kDa. After the repeated trials, the protein was completely denatured and depolymerized, which broke intra- and intermolecular hydrogen bonds and completely disrupted the secondary and tertiary structure of the protein molecule.

2) Loading: we ensured the regularity of the bands. To prevent oversaturation of HKPs, we performed several gradient tests and finally achieved a loading of 10 μg per well to ensure clear target bands and to ensure the HKPs were not overexpressed to the detriment of quantification.

3) Electrophoresis: the final setting was to electrophoresis at 120 V in ice. After reaching the separating gel, the voltage was turned to 140 -160 V till the blue line reached the bottom of the gel. It was ensured that this process was performed in the ice, reducing the distortion of the protein bands.

4) Transfer: it was ensured that the desired target proteins could be completely transferred from the gel to the PVDF membrane with a low energy transfer for 30 min, which was verified with the use of stain-free gel (Figure 5). By performing the current protocol, it was essentially ensured that proteins below 250 kDa could be successfully transferred to the membrane, leaving only part of the protein above 250 kDa remaining on the transferred gel (the proteins on the membrane after the transfer are presented in Figure 7 C).
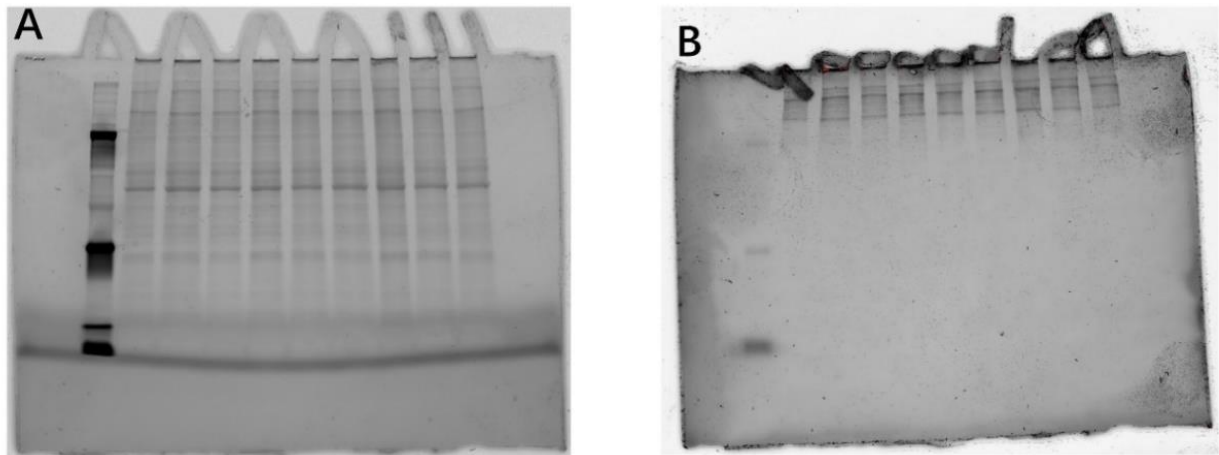
Figure 5: Detection of total protein on gel and membrane: (A) gel before transfer; (B) gel after transfer.

3.1.1 Loading control and housekeeper proteins

In the assessment of the results of Western blot, it should be ensured that the quantitative data originated from independent samples of an experiment and that it permits accurate quantification, and multiple factors should be considered to ensure the accuracy and quality of the blot. A critical factor is the equivalent protein load in the respective lane, which can vary depending on the protein concentration assay, loading volume, or transfer efficiency, and the amount of target protein should be corrected for the above-mentioned potential differences with the use of loading controls to correct for the amount of protein present in each lane. Since HKPs are relatively stable in tissue expression, they have been generally used as internal loading controls (83, 84).β-actin and 3-phosphoglycerate dehydrogenase (GAPDH) are the two most frequently applied loading controls (85). Thus, at the beginning of our Western blot protocol establishment, we selected β-actin and GAPDH as the loading control to permit accurate quantification.

Three of the HKPs (mouse anti-GAPDH, mouse anti-β-actin and rabbit anti-β-actin) were selected for testing. Moreover, since the later target proteins came to group host rabbit and host mouse antibodies, respectively, we selected HKPs of different genera to prepare for later multiple staining. We obtained the bands of HKPs in optimized conditions, and the target bands in the blots were regular and clear with low background, no ghosting and tailing. Figure 6 presents the results.
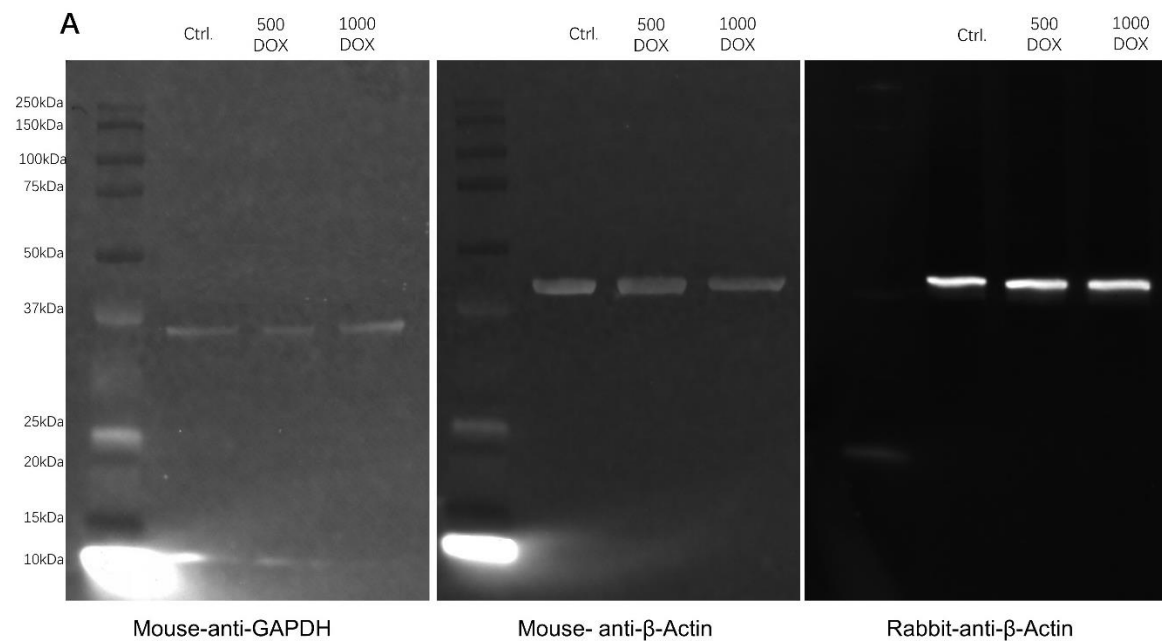
Figure 6: Different HKPs in blots: mouse anti-GAPDH, mouse anti-β-actin, rabbit anti-β-actin in blots were regular and clear with low background, no ghosting and tailing. Dilution concentration of primary Ab was 1:5,000, 4-20%gel, 10 μg protein per well.

3.1.2   Detection of total protein

Although HKPs in histology have a relatively consistent expression, the bands from our detection of HKPs indicated that different HKPs in the same cells had different expressions, and there could be slight differences in the expression of equivalent proteins in different stimulation groups as well. Thus, we planned to detect the total protein for further quantification. We applied two methods (i.e., stain-free gel and ponceau S staining) for total protein detection. Ponceau S is the conventional way of total protein detection, which has a relatively low cost and is simple to perform. However, it is affected by different external conditions, especially the time after staining (Figure 7 A, B). Accordingly, we preferred stain-free gel for total protein quantification. The stain-free bands were not dependent on the duration of staining or decolorization. The intensity of the bands on the stain-free blots was not reduced over time. Even when comparing the total protein bands on the membrane before and after blocking and immunostaining, no more pronounced decrement was reported (Figure 7 C, D).
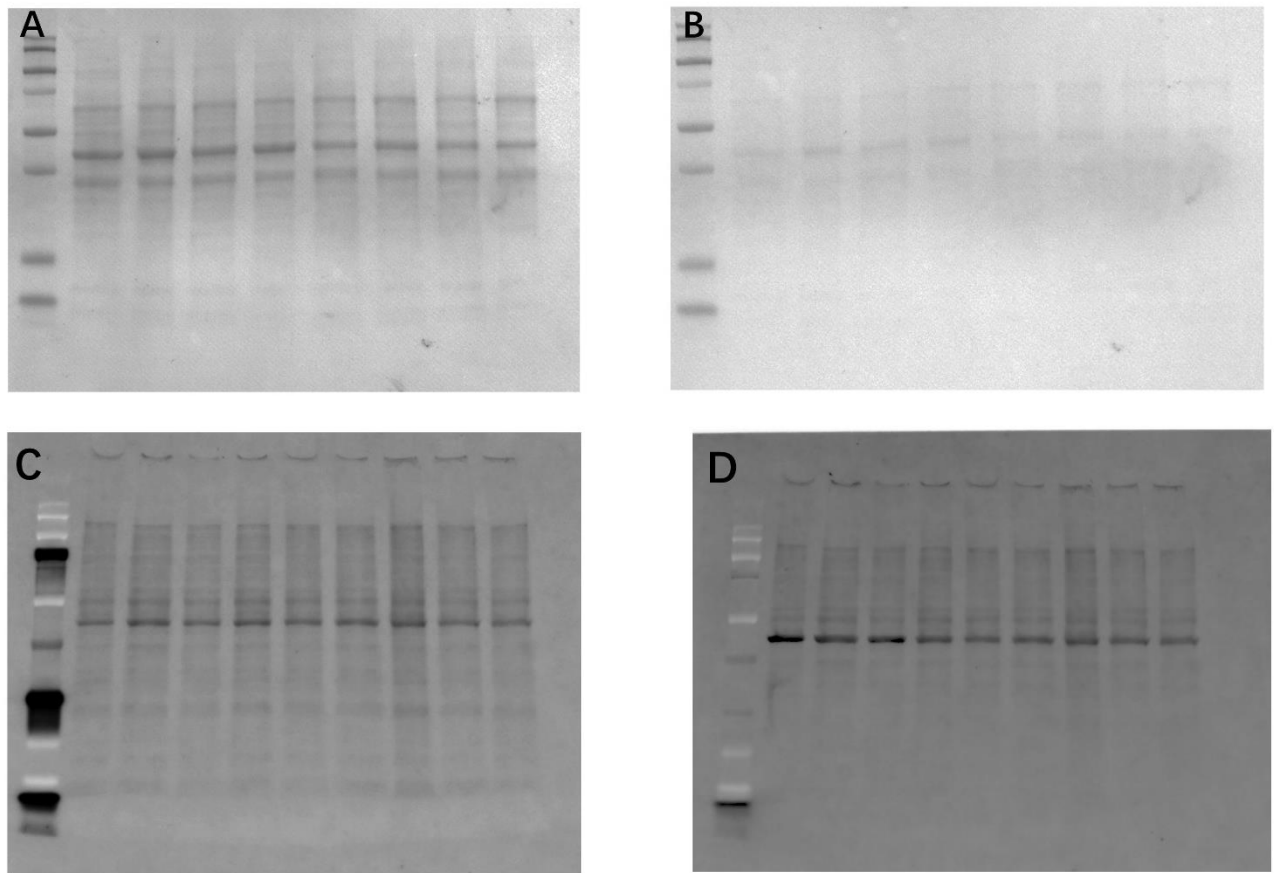
Figure 7: Total protein bands in blots: (A) Membrane after ponceau S staining is detected imme-
diately; (B) Membrane after ponceau S staining 10 min; (C) Membrane after transfer and before
blocking; (D) Membrane after blocking and immunostaining.

3.1.3 Multiplex blot for two target proteins

Using an optimized Western blot protocol combined with immunofluorescence Western
blot methods, we obtained the possibility of presenting multiple targets in one blot.

An optimized protocol and imaging modality should meet the requirements of conforming
the primary antibodies of different species (mouse, rabbit, goat or others) in combination
with secondary antibodies attached to different fluorochromes. In addition, the fluorescent
antibodies attached to the secondary antibodies should be in different channels. For the
specific wavelength and channel of fluorescent staining, the company's information
should be referenced. To establish multiple blots, we needed to create images of different
channels. After blocking, the PVDF membrane was incubated with primary and second-
ary antibodies. We aimed to achieve simultaneous incubation of at least two antibodies
that would not interfere with each other during imaging. For instance, for mouse anti-β-
actin (1:5,000) and rabbit anti-Bmp-2 (1:5,000), in which mouse anti-β-actin (1:5,000)

bound specifically to IgG-goat anti-mouse-Star Bright Blue 700 (1:2,500) and rabbit anti-Bmp-2 (1:5,000) bound specifically to goat anti-rabbit-Alexa Fluor 555 IgG (1:2,500); both secondary antibodies were coupled fluorescent dyes in special channels for imaging and visualized in special channels. The total protein uptake channel was the "stain free blot", which did not overlap with the channels above, so that the total protein channel could be incorporated into the image to give a richer multiplex result as well (Figure 8).

3.1.4 Targets for Western Blots

Total proteins from cells and vascular tissue were extracted and tested on various target proteins, some of which worked well with antibodies to the target proteins and some of which did not (Table 9), and all the antibodies, except for SIRT2, that were not in multiplot experiments, had high performance in multiple bolts.

Table 9: Target proteins for Western Blot

Target antibodies	Company and number	For cells	For tissue	Notes
Raabit-β-ACTIN	Santa cruz, sc-7210	√	√	
Mouse-β-ACTIN	Cell Signaling Technology, 8H10D10,	√	√	
Rabbit-GAPDH	Cell Signaling Technology, D4C6R	√	√	
Rabbit-Bmp-2	Abcam, ab214821,	√	√	
Rabbit-P21	Abcam, ab109199,	√	√	75kda,15kda specific bands for rVsmc, and bands for ex vivo tissue are very inconspicuous
Rabbit-RUNX2	Santa cruz, sc-10758	√	√	Some specific bands for rVsmc
Rabbit-ALP	Invitrogen, 7H11L3	√	√	50kda specific bands for rVsmc
Mouse-SIRT1	Abcam, ab110304,	√	--	
Rabbit-SIRT2	Abcam, ab211033,	√	--	Some specific bands for rVsmc.
Mouse-SIRT3	Abcam, ab246522,	x	--	
Goat-IL-6	Bio-Rad, AAR35	x	x	
Rabbit-IL-1β	Bio-Rad, AAR15G	x	x	

√, works with positive control; X, no bands; --, was not tested
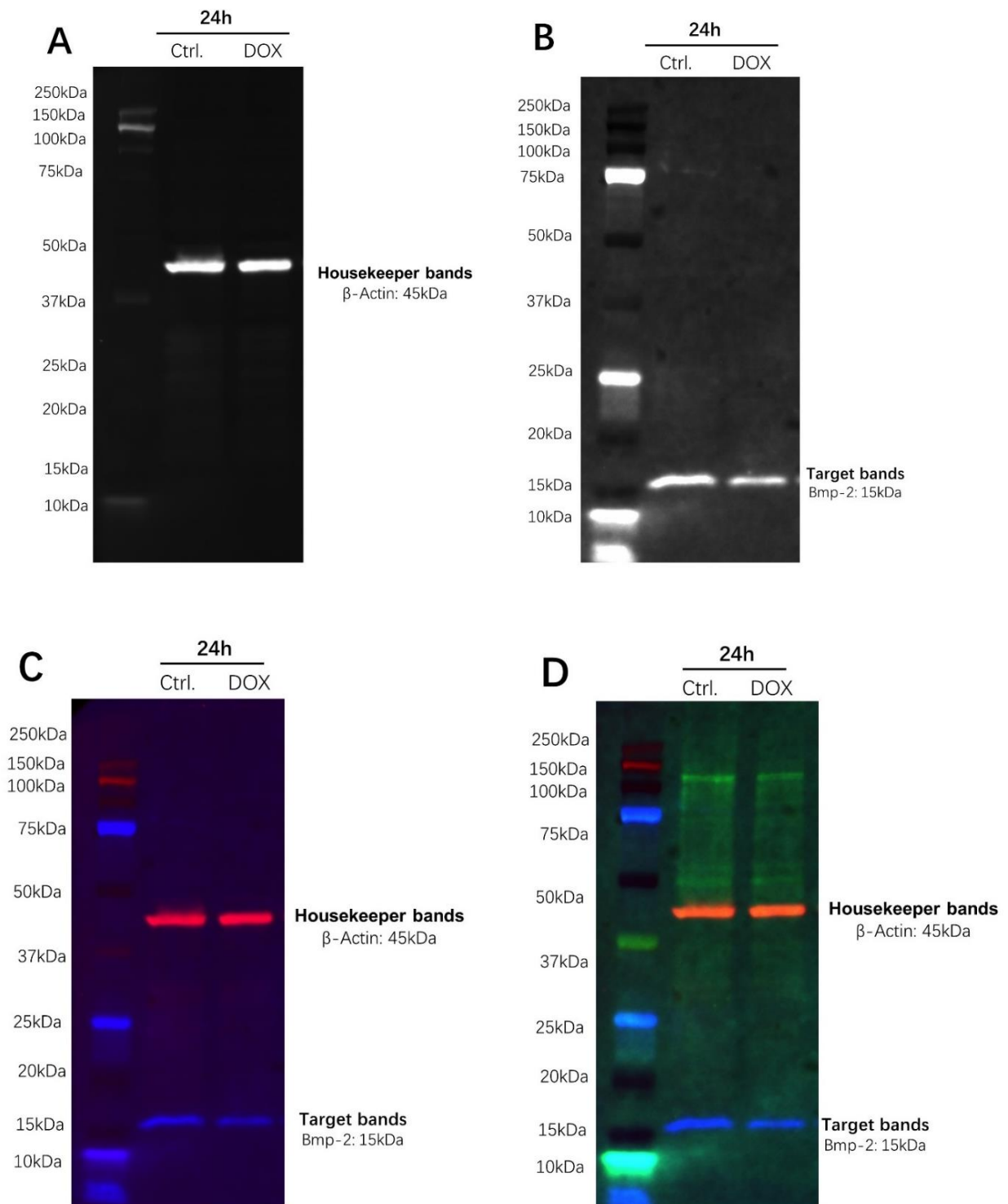
Figure 8: Multiplex blot for two target proteins (merge)**:** (A) Only mouse anti-β-actin (1:5,000) + StarBright Blue 700 goat anti-mouse IgG, detected in the "Bright Blue 700" channel; (B) Only rabbit anti-Bmp-2 (1:5,000) + goat anti-rabbit-Alexa Fluor 555 IgG, detected in the "Alexa Fluor 546" channel; (C) Merge channel "Bright Blue 700" (Red) and "Alexa Fluor 546" (Blue). (D) Merge channel "Bright Blue 700" (Red), "Alexa Fluor 546" (Blue) and "stain free blot" channel (Green). All secondary antibodies at 1:2500 dilution.12% Stain-free gel, 10ug protein per well.

3.2   Detection of calcification and senescence in vitro

3.2.1   Established in vitro model

In this paper, we used high phosphorus (Pi) medium to investigate whether high phosphorus concentrations directly stimulate VSMCs and arterial tissue to cause calcification. In comparison with control cells, calcification of VSMCs was significantly increased after 14 d of exposure to high phosphorus medium. In parallel, when DOX was added to the high phosphate medium, calcification increased and was significantly higher than in the blank high phosphate group when added at 100 nmol/l as indicated by Alizarin red S staining (Figure 9). By contrast, no mineral deposition was detected in the control medium.
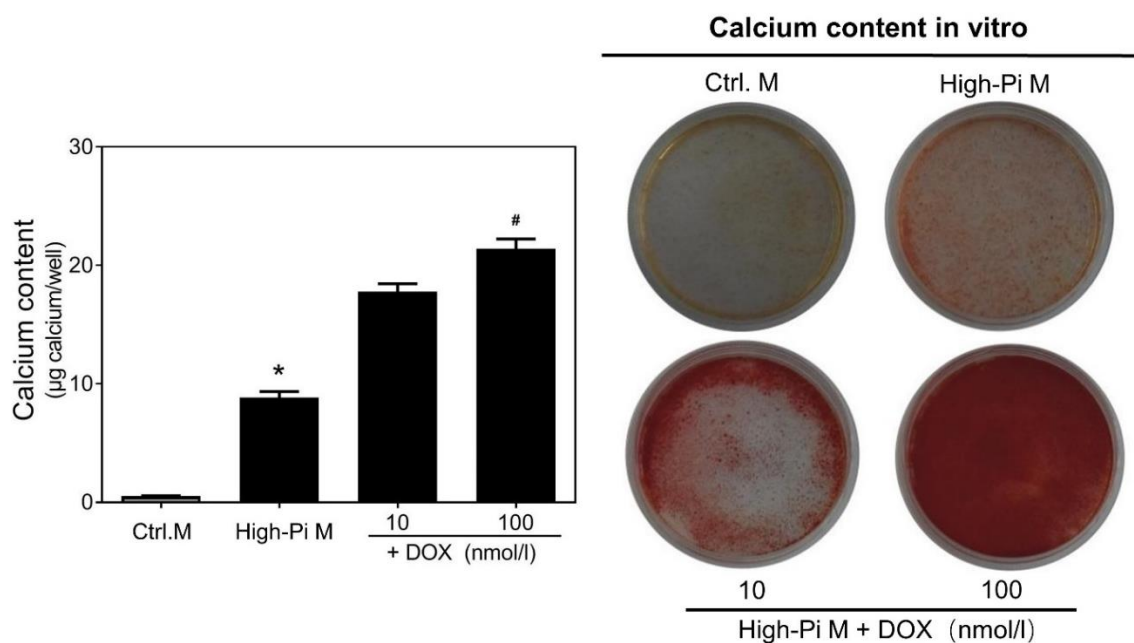
Figure 9: High phosphate medium and DOX promoted calcification: High phosphate concentrations facilitated calcification in vitro. VSMCs were exposed to control medium, high-Pi medium, high-Pi medium+10 nmol/l or high-Pi medium+100 nmol/l for 14 d, and Alizarin red staining was performed to visualize calcification. *P<0.05 vs control; #P<0.05 vs High-Pi medium. The results partially reference our publication (86).

3.2.2   p21 upon DOX stimulation

Since p21 is the classical senescence pathway, we aimed to determine whether there is a correlation between VSMCs and the p21 senescence pathway. First, we stimulated VSMCs by DOX to clarify whether there is an activation of p21. According to the results of qPCR, the mRNA expression of the senescence marker p21 was significantly higher

in VSMCs cells stimulated by DOX than in the control cells (Figure 10 A). After conducting an optimized protein measurement, we started to explore the protein level. Next, we examined p21 protein expression levels and found that p21 expression also tended to increase in DOX-stimulated VSMCs in comparison with control cells under DOX stimulation (Figure 10 B). Overall, the above-mentioned findings suggest that p21 is involved in DOX-stimulated VSMCs senescence and validated at the translational level.
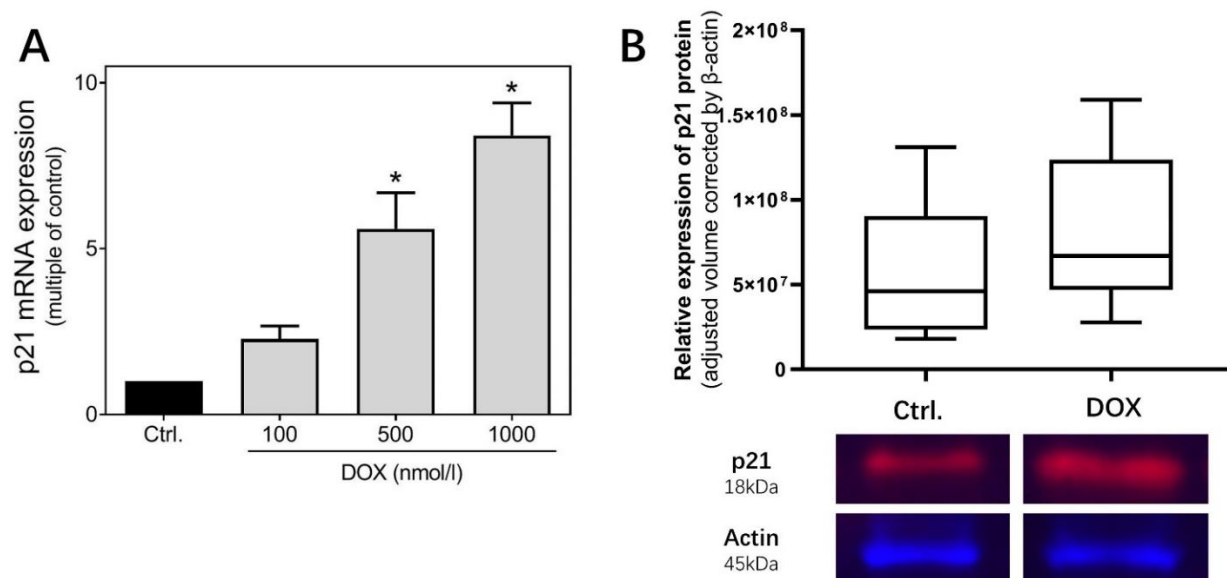
Figure 10: Expression of p21 by stimulation with doxorubicin: DOX stimulation induced high expression and protein of p21: (A) VSMCs were stimulated with quiescence medium (Ctrl.), 100 nmol/l DOX, 500 nmol/l DOX or 1000 nmol/l DOX for 48h, and mRNA expression of p21 was measured through quantitative real-time qPCR. (B) VSMCs were stimulated with control medium (Ctrl.) or 1000 nmol/l DOX for 48h, and protein expression of p21 was measured with Western blot. Blots were developed using rabbit anti-p21 (1:2500) + IgG-goat anti-rabbit-StarBright Blue700 (1:2500) (red), as well as mouse anti-β-actin (1:5,000) + IgG-goat anti-mouse-StarBright Blue520 (1:2500) (blue), with 10ug protein per well. Blots showed a representative experiment section of n≥3. The results partially reference our publication (86).

3.2.3 Detection of ALP and Cbfa1 upon DOX stimulation

We analyzed the induction of DOX at the genetic level using qPCR, finding that mRNA expression of the markers ALP and Cbfa1 was significantly higher in VSMCs cells under DOX stimulation than in the control (Figure 11 A, 12 A). Likewise, Western blot validation at the protein level achieved the same results (Figure 11 B, 12 B).

Figure 11: Expression of ALP by stimulation with doxorubicin: (A) VSMCs were stimulated using quiescence medium (Ctrl.), 100 nmol/l DOX, 500 nmol/l DOX or 1,000 nmol/l DOX for 72 h, and mRNA expression of ALP was measured with quantitative real-time qPCR. The picture shows a representative experiment section of n≥3. Data were expressed as means ± SEM. n≥3, *p<0.05 vs. control. (B) VSMCs were stimulated with control medium (Ctrl.) or 1,000 nmol/l DOX for 48 h, and protein expression of ALP was measured with Western blot. Blots were developed with rabbit anti-ALP (1: 500) + IgG-goat anti-rabbit-StarBright Blue700 (1:2,500) (red), as well as mouse anti-β-actin (1:5,000) + IgG-goat anti-mouse-StarBright Blue520 (1:2,500) (blue), with 10 µg protein per well. Blots showed a representative experiment section of n≥3. The results partially reference our publication (86).
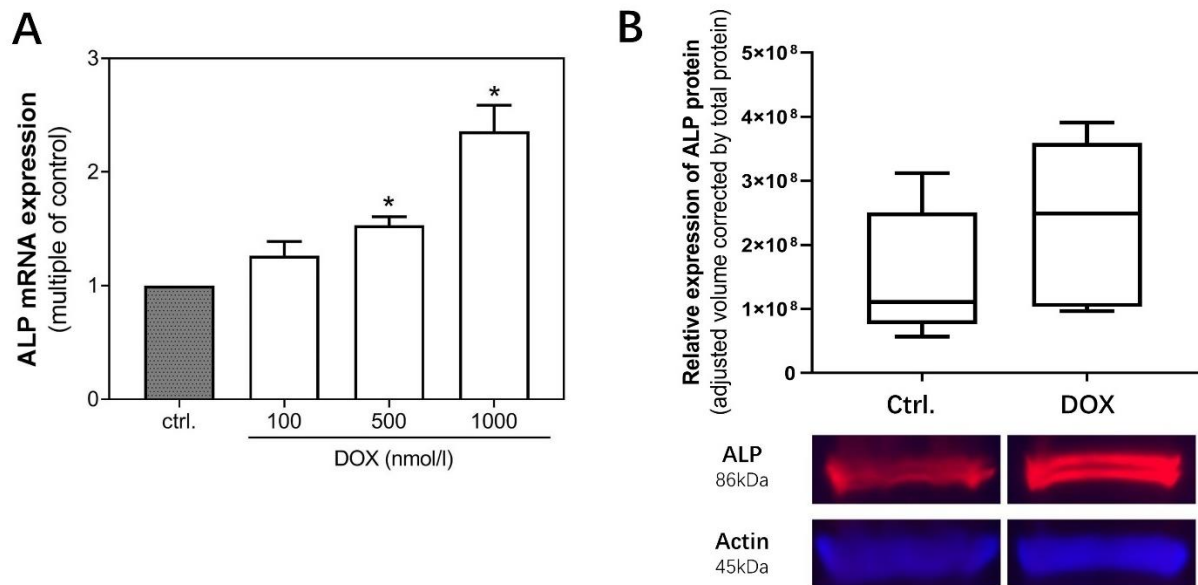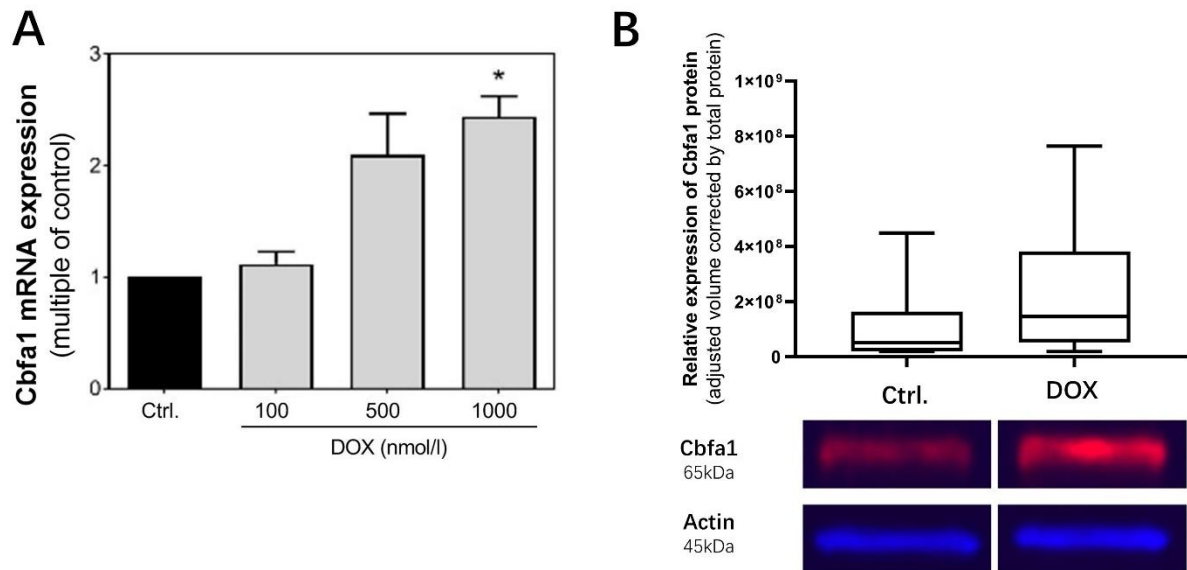
Figure 12: Expression of Cbfa1 by stimulation with doxorubicin: (A) VSMCs were stimulated using quiescence medium (Ctrl.), 100 nmol/l DOX, 500 nmol/l DOX or 1,000 nmol/l DOX for 48 h, and mRNA expression of Cbfa1 was measured with quantitative real-time qPCR. The picture shows a representative experiment section of n≥3. Data were expressed as means ± SEM. n≥3, *p<0.05 vs. control. (B) VSMCs were stimulated with control medium (Ctrl.) or 1,000 nmol/l DOX for 48h, and protein expression of Cbfa1 was measured with Western blot. Blots were developed with rabbit anti-Runx2 (1:1,000) + IgG-goat anti-rabbit-StarBright Blue700(1:2,500) (red), as well as mouse anti-β-actin (1:5,000) + IgG-goat anti-mouse-StarBright Blue520 (1:2,500) (blue), with 10 µg protein per well. Blots showed a representative experiment section of n≥3. The results partially reference our publication (86).

3.3   Detection of calcification in ex vivo model

3.3.1   Establishment of vascular calcification ex vivo model

The calcification ex vivo model was also validated by quantifying the calcium content of aortic rings as significantly higher than controls after 14 d of stimulation and assessing the localization of calcification with alizarin red staining (Figure 13). The above results show that this paper successfully constructed an ex vivo model of VC by exposure to high phosphorus conditions. Moreover, samples from a new ex vivo method of the isolated-perfused aorta (IPA) that was recently developed by our team were included in the Western blot detection of current study.

Our existing studies have confirmed that when using intravascular measurement of perfusion medium for 14 d, both H/E and Alizarin red staining showed significant mineralization of the vessel wall in the perfused high phosphorus medium group in comparison with the perfused control medium (87).
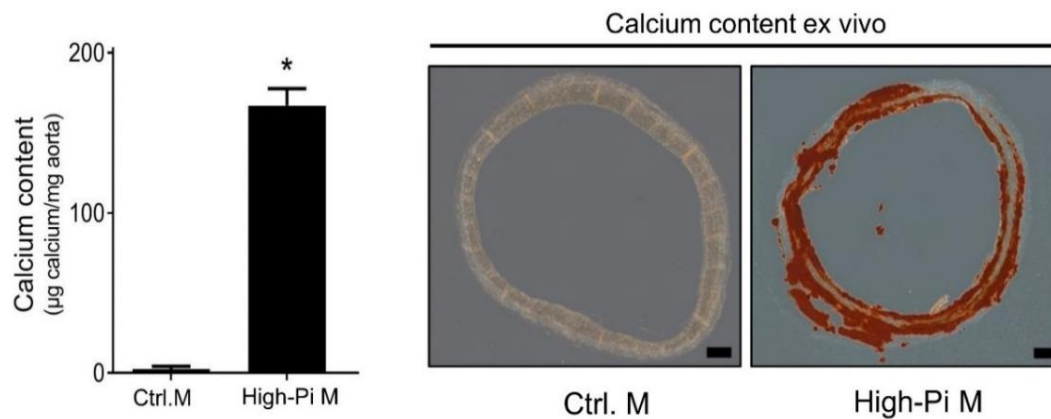
Figure 13: High phosphate medium promoted calcification in ex vivo: Aortic rings were cultured in either control or high-Pi medium for 14 days, and the calcium content was determined with Alizarin red S staining, which showed a significant increase in high-Pi medium (P <0.05). The results partially reference our previous publication (86).

3.3.2 Quantification of proteins in tissues

After establishing the ex vivo calcification model, we explored its correlates of aging and calcification. As reported by existing studies, aortic tissue induces calcification following IPA and the expression of relevant indicator mRNAs in the tissue was measured (87), and then protein expression in the tissue was quantified.

To confirm the osteoblastic transition and senescence of aortic cells, p21, Cbfa1 and ALP were examined using Western blot. As revealed by the Western blot result, p21 protein expression was higher in isolated arterial rings in high phosphorus medium than in the control (Figure 14 A). High phosphate medium also increased the trend of both ALP (Figure 15 A) and Cbfa1 (Figure 14 B) protein expression within isolated arterial rings. Consistently to our previous detection of ALP mRNA expression in IPA tissue (87), arteries perfused with high phosphate in IPA exhibited higher ALP expression when compared with the control (Figure 15 B).
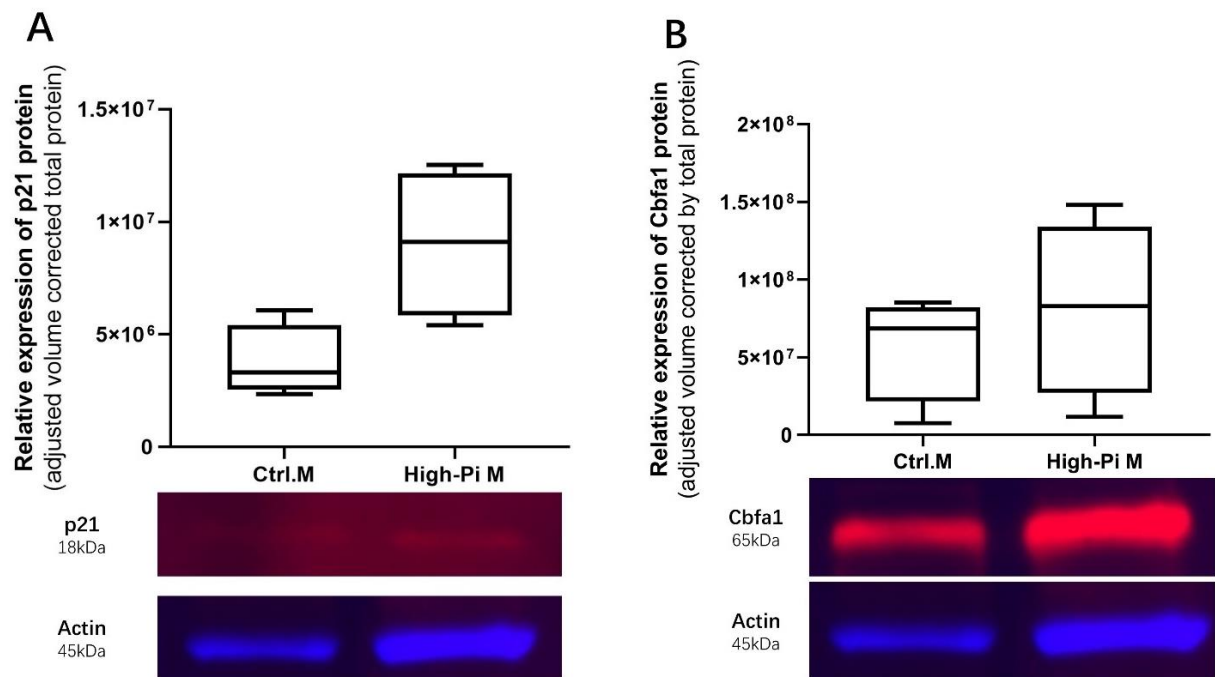
Figure 14: Protein expression of p21 and Cbfa1 by stimulation with high-phosphate medium ex vivo**:** We cultured aortic rings using either control (Ctrl.) or high-phosphate (High-Pi) medium for 14 d; (A) Protein expression of p21 was measured using Western blot. Blots were developed with rabbit anti-p21 (1:2,500) + IgG-goat anti-rabbit-StarBright Blue700 (1:2,500) (red), as well as mouse anti-β-actin (1:2,500) + IgG-goat anti-mouse-StarBright Blue520 (1:2,500) (blue). (B) Protein expression of Cbfa1 was measured with Western blot. Blots were developed with rabbit anti-Runx2 (1:2,500) + IgG-goat anti-rabbit-StarBright Blue700 (1:2,500) (red), as well as mouse anti-β-actin (1:2,500) + IgG-goat anti-mouse-StarBright Blue520 (1:2,500) (blue), with 10ug protein per well. Blots showed a representative experiment section of n≥3.
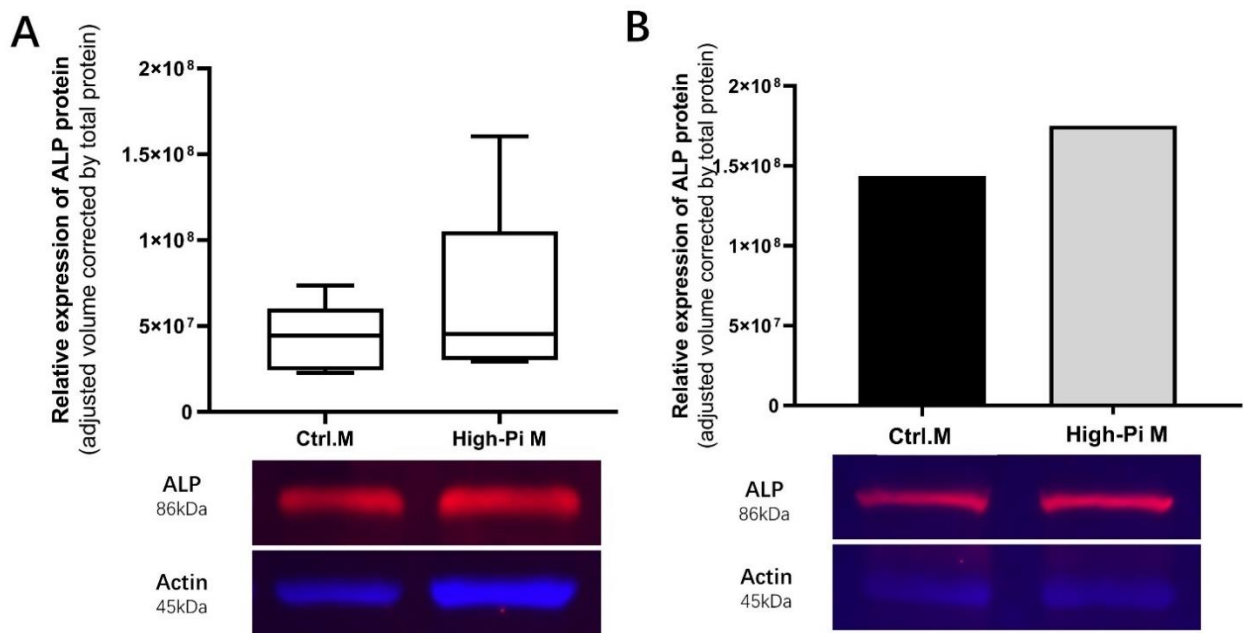
Figure 15: Protein expression of ALP in aortic tissue**:** (A) We cultured aortic rings using control (Ctrl.) or high-phosphate (High-Pi) medium for 14 d, and measured the protein expression of ALP using Western blot. Blots were developed with rabbit anti-Runx2 (1:2,500) + IgG-goat anti-rabbit-StarBright Blue700 (1:2,500) (red), as well as mouse anti-β-actin (1:2,500) + IgG-goat anti-mouse-StarBright Blue520 (1:2,500) (blue). Blots showed a representative experiment section of n≥3, with 10 μg protein per well; (B) Comparison of ALP protein expression in aortic tissue after perfusion for 7d with a control medium (Ctrl.) and high-phosphate (High-Pi). Blots were developed with rabbit anti-Runx2 (1:2,500) + IgG-goat anti-rabbit-StarBright Blue700 (1:2,500) (red), as well as mouse anti-β-actin (1:2,500) + IgG-goat anti-mouse-StarBright Blue520 (1:2,500) (blue), with 15 μg protein per well.

4. Discussion

VC refers to a widespread vascular pathology showing significant relationships to diseases (e.g., CKD, diabetes mellitus, hypertension, and atherosclerotic heart disease). In most cases, patients with calcification are at elevated risks of adverse cardiovascular events and death, with an even greater increase in the risk of the above-mentioned associations in patients with CKD. Existing diagnostic and therapeutic methods for VC have been relatively limited. For this reason, gaining more insights into the underlying pathological mechanisms of VC and early intervention may be more effective strategies for VC treatment. However, vascular tissue in animals is limited, and we obtained a small amount of vascular tissue in rats or mice, so being able to obtain more targets with a lower amount of tissue protein would lead to a much better result. Thus, the first part of this paper establishes a reasonable Western blotting protocol that could detect multiple target proteins simultaneously based on fluorescence detection and add total protein detection, which could provide better quantification. Since existing studies reported that senescence and secreted SASP may be involved in VC in CKD patients, the second part of this paper explored the activation of senescence signaling (p21). Lastly, since calcification studies cannot be conducted directly in humans, exploring a more appropriate model of calcification that meets the 3Rs principle, as well as preliminarily exploring the role of senescence factor p21 and some biochemical markers for calcification (Cbfa-1 and ALP) was in the third part of this paper.

4.1 Optimization and quantification in Western Blot

Western blotting has been a widely used method to quantify protein levels, and it is available to accurately semi-quantify the quantitation of specified proteins in complex samples. Thus, for nearly three decades, HKPs, highly abundant in the samples and capable of serving as representatives of the entire protein population, have been extensively used to select lane normalization to correct for errors related to variations in sample loading and transfer (88-90).

However, as clarified by recent studies, the above-mentioned HKPs had some limitations in serving as loading controls, and the three common HKPs (β-actin, GAPDH and β-tubulin) differed significantly in different tissues or disease states under many conditions (84, 91). Besides, because of the high abundance of HKPs, when the target proteins are

less expressed (e.g., the secreted proteins in our experiments), we would load more total protein, which would lead to an overload of abundant HKPs. Moreover, GAPDH and Actin in most experiments were prone to oversaturation when used as loading controls, which could affect the final standardization (84). Accordingly, the immediate effect of poor normalization is evident, so the purpose of data standardization cannot be met. Over the past few years, the total density of blotted transferred proteins has been demonstrated as a means of standardizing data, and there are various stains available for visualizing, imaging and quantifying proteins transferred on blots (e.g., ponceau S, deep purple and the stain-free system), and it has been found to be a better normalization control than HKPs for several cells and tissues (92, 93). This paper used the protocol with total proteins and HKPs as the loading controls, so normalization was no longer dependent on the expression of a single protein and they could be validated against each other to achieve the optimal results. In the establishment of the protocol, we used ponceau S staining staining and Stain-free gel to detect total proteins. To be specific, ponceau S is the most common total protein stain with the highest sensitivity for protein detection, and using ponceau S is an easy and inexpensive way to detect total proteins, which is characterized by simple handling and reversible staining (94, 95). However, according to our results, the strength of the stained bands decreased significantly over time when membranes were stained with ponceau S, which increased the difficulty in handling and caused poor color development and substandard quantification if the staining was not done in a timely manner (96). We proceeded to use stain-free precast gels, which could also be a fast and simple method to detect proteins in the gels before and after transfer. On the one hand, the transfer of proteins from gel to the membrane could be verified. On the other hand, this staining method could be stable, unaffected by time extension, containment and immunoassay, which is a very well-established method for measuring total protein. The prominent total protein bands and high-quality images obtained by our experiments using the stain-free method prompted us to determine the suitability of the method as a loading control for the blots of VSMCs protein (vascular tissue by the InventTM extraction method) commonly performed in our Western blot.

4.2   Modeling and optimization for the study of calcification

Since the precise underlying mechanisms of VC have not been clarified thus far, researchers have mostly resorted to in vitro and in vivo models of VC for a more in-depth

mechanistic comprehension of the VC process. Our team previously summarized the current cellular and animal models (70, 97) applied for VC research by review, and the VC model formed in this paper benefited from previous experience. The investigation of VSMCs osteogenic transition is considered as one of the most extensive in vitro studies, whereas VSMCs do not in general calcify spontaneously and require calcification stimulation before the formation of a VC model. In this paper, we also built in vitro models after the stimulation of VSMCs with high phosphorus medium for 14 d after the calcification model.

The extraction of cellular proteins for Western blot with the use of extracted VSMCs in in vitro studies is an essential part of the current study. With the multiple staining Western blot in this study, we could achieve multiple target proteins in one blot. In other words, we visualized the variations of multiple parameters in one blot. The tissue organization of cells is lost in cell models in vitro and processes involving cooperative interaction with the extracellular matrix cannot be well investigated. Thus, animal models have been established for the assessment of VC. Models using the in vitro environment of aortic tissue to simulate the induced in vivo environment are termed in vitro models, which are capable of simulating different aspects of the pathophysiological mechanisms involved in the VC process. This paper also used an ex vivo arterial model mimicking the calcification induced by a high phosphorus environment in vivo. Additionally, our group published a methodology nearer to the in vivo physiological environment, i.e., IPA, in which the high phosphate medium only contacts and stimulates the lumen and endothelium of the aortic vessels, recreating the hyperphosphatemic state in vivo. This model can overcome the disadvantage that in vitro models do not involve cooperative interactions with the extracellular matrix (ECM) (87), and it is closer to the physiological environment of human VC than a purely in vitro model. However, the size of ex vivo tissues (e.g., incubated arterial rings or IPA tissues) was minimal, and usually only 3-5 mg of tissue was available for the experiment, and in the case of mouse arteries, even smaller amounts of less than 1 mg. According to the previous typical protocol for Western blot, protein quantification would require considerable tissue for experiments. Using the improved tissue protein extraction method and the improved Western blot protocol, we were able to analyze multiple parameters in a single blot even with 5 mg of tissue, saving the amount of tissue and meeting the experimental needs. This protocol was also suitable for animal tissues and reduced the number of animals required, which is another aspect of the 3R principle (98).

4.3   Cellular senescence and p21 pathway for vascular calcification in vitro and ex vivo

Cellular senescence is a state of permanent proliferation arrest which is accompanied by cell morphology, function and metabolism variations, and even cell phenotype variations (99). Senescent cells can impair functions, while affecting surrounding cells and tissues based on different mechanisms, thereby causing tissue dysfunction. According to a growing number of in vivo and in vitro studies, cellular senescence is of high importance to the development of related diseases (100-102). VSMC senescence is closely related to the development of atherosclerosis. According to Noureddine et al., pulmonary artery smooth muscle cell senescence is a central mechanism in the development of pulmonary hypertension in chronic lung disease (103). Moreover, VSMC senescence facilitates atherogenesis and increases atheromatous plaque instability (104). The importance of VSMC senescence in the pathogenesis of relevant cardiovascular diseases has been well confirmed. However, the mechanisms underlying the progression of disease due to VSMC aging remain unclear. DOX, a compound belonging to the anthracycline family, is found as a common anticancer drug, which is widely applied in chemotherapy for various cancers. DOX induces cellular senescence by different mechanisms (e.g., the ability of proteins involved in DNA replication and transcription to embed in the DNA helix and/or bind), thereby inhibiting: macromolecular synthesis; oxidative stress-induced free radical production, leading to leading to DNA damage and/or lipid peroxidation; and, alteration of decapping enzyme activity and induction of DNA damage by inhibiting topoisomerase II (105, 106). It can also induce cellular senescence and apoptosis directly through cytotoxic mechanisms including interference with its nuclear, autophagy, calcium stability and nitric oxide synthase activities as well as mitochondrial dysfunction (107, 108). Accordingly, Adriamycin has been commonly considered as an essential factor in the induction of cellular senescence.

Consistently with existing studies (109), p21, a classical pathway of the senescence pathway, may impact the regulation of the senescence process in VSMCs. p21 is capable of inhibiting cell proliferation directly by binding which inhibits cyclin-CDK complexes (110) and PCNA, or indirectly at the transcriptional level (111). p53 has been found to be the main activator of p21 transcription. p21 contains two conserved P53 response elements in its promoter (112). Different stresses (e.g., DNA damage and oxidative stress) up-

regulate p53 activity, thereby leading to p21 expression (113). Considerable numbers of inflammatory cytokines, tumor suppressors and nutrients are capable of inducing p21 transcription (114). Furthermore, several studies reported that p21 can promote apoptosis and activate autophagy to accelerate cell death in cancer cells (115). As identified in senescent human diploid fibroblasts, p21 is capable of further inducing senescence in normal cells. Under cell cycle arrest or considerable withdrawal, cells enter a quiescent or senescent state, which is usually accompanied by up-regulated p21 expression (116). According to other in vitro experiments, senescent VSMCs, like other cells, are accompanied by DNA damage and loss of telomeres, the expression of the cell cycle protein-dependent kinase inhibitor p21, as well as the expression of Sa-β-Gal (117). According to existing studies, senescence of VSMCs can induce osteoblast-like transformation (118). In this paper, we induced senescence of VSMCs after short-term stimulation using DOX as an inducer. After DOX Stimulation, in comparison with unstimulated VSMCs, the cells in the DOX group became flattened and enlarged, with clearly visible sarcomeres typical of senescent cells. Moreover, in a parallel study in our group, H2AX and β-gal staining of VSMCs were elevated after DOX stimulation, indicating the development of senescence in VSMCs after DOX stimulation.

Additionally, this costimulation of calcification was significantly increased when superimposed with graded concentrations of DOX in a high phosphate medium. The results of Alizarin red staining and calcium content quantification revealed that VSMCs in the DOX group had a more pronounced calcification than cells in the non-DOX group, and that the extent of VSMC calcification in vitro increased in a dose-dependent manner with DOX. The senescence-associated p21 gene and protein were both up-regulated in VSMCs after DOX induction, with a significant difference in the upward trend after 48 h.

To further validate the generality of the correlation between cellular senescence and calcification, we analyzed the correlation between hyperphosphate-induced senescence and calcification in vascular tissue as well. We observed a trend towards increased p21 protein expression in the high phosphate group in comparison with normal controls ex vivo, which was confirmed by existing studies on the correlation between the senescence pathway and vascular calcification. p21, a key proponent downstream of p53, has been found as a vital regulator of the cell cycle checkpoint, and it is of high importance to G2/M transition and mitotic progression (119, 120). p21 is involved in several critical roles in

apoptosis, differentiation, DNA repair, transcription as well as cell migration for apoptosis, differentiation and reprogramming (121). Moreover, the calcification of the middle layer of aortic explants was induced when phosphate concentrations in the medium mimicked hyperlipidemic conditions, and this calcification was related to fibrosis and apoptosis-related media calcification (25), which revealed that high phosphorus-induced calcification of the media of the aortic rings may be involved in the fibrosis and the apoptosis, and may be subordinate to cellular transdifferentiation of the osteoblast phenotype (122). As reported by a wide range of existing studies, hyperphosphate is of high importance to the mechanisms of VC (123-125). Most of the existing ex vivo systems of studying VC cover the use of high concentrations of phosphate, for which phosphate is confirmed as a fundamental parameter (87, 126). As confirmed by existing studies, phosphate-induced oxidative stress can be transduced via multiple downstream signaling pathways to mediate osteogenesis/chondrogenesis and calcification in VSMCs, which includes the promotion of osteoinduction in VSMCs via the ERK1/2 map-kinase (127) and the p38 Map-kinase pathway (128), as well as the activation of nuclear factor kappa-light-chain-enhancer of activated B cells (NF-κB) (129) and NF-κB-dependent osteoinductive signaling pathways (130), which promote inflammatory responses in VSMCs and further promote calcification. Oxidation is of high importance to cellular senescence, with senescent VSMCs achieving higher levels of ROS than young VSMCs (52). High levels of ROS may cause DNA damage response pathways that activate p53/p21 effector proteins by NF-κB signaling, inducing senescence in VSMCs (131), as well as ROS generation resulting in loss of mitochondrial function (132) and telomere shortening (133), which further facilitates cellular senescence.

4.4 Biomarkers of Vascular Calcification

Osteoblastic transformation of VSMCs and induction of calcification in ex vivo was confirmed by detecting calcification-related regulators. In this paper, significantly higher calcification indices (Alizarin red staining and quantification of calcium content) were found in DOX-induced VSMC and high phosphorus-induced isolated vascular tissues than in the controls, accompanied by the up-regulated expressions of related regulators ALP and Cbfa1.

Cellular senescence induced by DOX or high phosphorus stimulation leads to permanent cell cycle stagnation and may stimulate the secretion of various SASPs, whereas the

presence of SASPs accelerates the senescence-associated calcification (56, 134) and up-regulates several bone-related transcription factors, as well as their relevant bone and chondrocyte proteins. To be specific, Cbfa1, i.e., Runt-related transcription factor 2 (Runx2), can activate and initiate the differentiation of bone marrow mesenchymal stem cells (MSCs) into osteoblasts and regulate osteoblast maturation, thereby controlling intramembranous and endochondral osteogenesis (135). Cbfa1 knockout mice did not form mineralized bone and had significant skeletal defects (136), which could be a specific transactivator of osteoblastogenesis as well as differentiation and the initiator of differentiation of MSCs into osteoblasts (137, 138). According to in vitro studies, high phosphorus levels in extracellular cells actuated VC after entering smooth muscle cells via Napi transport/Pit-1 in blood-weeping smooth muscle cells and up-regulating Cbfa1 expression. High phosphorus culture of VSMCs inhibited the activation of Pit1, while blocking the expression of Cbfa1 by small interfering RNA (siRNA) (139). In this experiment, we used high phosphorus medium to induce aortic ring tissue, through which an ex vivo model of calcification was built. Arterial rings in high phosphorus medium showed higher calcium deposition and expressed more Cbfa1.

Some bone-related molecules, located downstream of Cbfa1, up-regulate the expressions of other bone-associated proteins, including osteocalcin and ALP (140-142). ALP is a functional phenotypic marker of osteoblasts, whereas its activity has been commonly exploited as a molecular marker of vascular calcification, which has a biological role in mineralization in vitro by releasing free phosphorus during β-glycerophosphate hydrolysis (143). During endochondral ossification, through hydrolysis of pyrophosphate, ALP activity is of high significance to hydroxyapatite formation, which generates the necessary phosphate for hydroxyapatite formation by similarly reducing inhibition of PPi crystallization (144). The activity of ALP was consequently confirmed to be critical to bone mineralization. In our present experiment, the up-regulated vascular ALP expression in vitro under high phosphate conditions was further confirmed with the use of Western blot as well. In addition, this experiment revealed an elevation of ALP in the high phosphorus group through an optimized IPA calcification model. Based on the up-regulated vascular ALP expression in the CKD mice model, we hypothesized that high phosphorus has a significant effect on VC in mice with CKD. It is also assumed that high phosphorus may be involved in the development of VC by up-regulating of ALP expression. In another parallel experiment by our group, female DBA2/N mice fell into 2 groups: one group was fed an

adenine-rich diet supplemented with 0.2% adenine, 6% protein, 1% calcium and 1% phosphate to successfully build a CKD mouse model; mice in the other group were provided with a similar diet without adenine and served as a normal control. In this paper, mRNA and protein levels of ALP were increased in the adenine-fed CKD mice. It was reported that renal failure up-regulates ALP expression in vascular smooth muscle, a process initially considered to promote calcification by providing inorganic phosphate from organic phosphate, but later found to be related to the hydrolysis and reduction of extracellular pyrophosphate levels. Mice deficient in ALP had up-regulated levels of pyrophosphate and mineralization defects (145). In vivo, the above-mentioned can be corrected by crossing them with mice defective in extracellular pyrophosphate production due to the absence of extracellular nucleotide pyrophosphorylase or the putative pyrophosphate translocator protein Ank (146). Accordingly, the overexpression of ALP induced ectopic calcification, further increasing the actions of VC (147).

5.   Conclusions

A multiplex Western blot protocol was developed, which is not only more time-efficient than the normal Western blot protocol, but which can detect multiple target protein bands (up to three) from different complementary interference channels, and the final result can merge one single blot. Besides quantification of HKPs, total protein quantification for validation enables more accurate detection of protein levels. This protocol also has the advantage that multiplex can be performed when having less material such as mice aortic tissue.

Using this new protocol, the protein expression level of several osteogenic proteins such as ALP, Cbfa1 and senescence protein as p21 could be detected in calcified VSMCs and calcified aortic tissue. Additionally, we preliminarily explored the VC process involved in the senescence pathway.

Reference list

1.   Lupo MG, Biancorosso N, Brilli E, Tarantino G, Adorni MP, Vivian G, Salvalaio M, Dall'Acqua S, Sut S, Neutel C, Chen H, Bressan A, Faggin E, Rattazzi M, Ferri N. Cholesterol-Lowering Action of a Novel Nutraceutical Combination in Uremic Rats: Insights into the Molecular Mechanism in a Hepatoma Cell Line. Nutrients. 2020;12(2).

2.   Rogers MA, Aikawa E. Cardiovascular calcification: artificial intelligence and big data accelerate mechanistic discovery. Nature reviews Cardiology. 2019;16(5):261-74.

3.   Gao J, Zhang K, Chen J, Wang MH, Wang J, Liu P, Huang H. Roles of aldosterone in vascular calcification: An update. European journal of pharmacology. 2016;786:186-93.

4.   Lin X, Li F, Xu F, Cui RR, Xiong D, Zhong JY, Zhu T, Shan SK, Wu F, Xie XB, Liao XB, Yuan LQ. Aberration methylation of miR-34b was involved in regulating vascular calcification by targeting Notch1. Aging. 2019;11(10):3182-97.

5.   Lanzer P, Hannan FM, Lanzer JD, Janzen J, Raggi P, Furniss D, Schuchardt M, Thakker R, Fok PW, Saez-Rodriguez J, Millan A, Sato Y, Ferraresi R, Virmani R, St Hilaire C. Medial Arterial Calcification: JACC State-of-the-Art Review. Journal of the American College of Cardiology. 2021;78(11):1145-65.

6.   Lacolley P, Regnault V, Laurent S. Mechanisms of Arterial Stiffening: From Mechanotransduction to Epigenetics. Arteriosclerosis, thrombosis, and vascular biology. 2020;40(5):1055-62.

7.   Lee HY, Park UJ, Kim HT, Roh YN. The Effect of Severe Femoropopliteal Arterial Calcification on the Treatment Outcome of Femoropopliteal Intervention in Patients with Ischemic Tissue Loss. Vascular specialist international. 2020;36(2):96-104.

8.   Lioufas NM, Pedagogos E, Hawley CM, Pascoe EM, Elder GJ, Badve SV, Valks A, Toussaint ND. Aortic Calcification and Arterial Stiffness Burden in a Chronic Kidney Disease Cohort with High Cardiovascular Risk: Baseline Characteristics of the Impact of Phosphate Reduction On Vascular End-Points in Chronic Kidney Disease Trial. American journal of nephrology. 2020;51(3):201-15.

9.   Jagieła J, Bartnicki P, Rysz J. Selected cardiovascular risk factors in early stages of chronic kidney disease. International urology and nephrology. 2020;52(2):303-14.

10.   Chen NX, Moe SM. Vascular calcification: pathophysiology and risk factors. Current hypertension reports. 2012;14(3):228-37.

11.   Rennenberg RJ, Kessels AG, Schurgers LJ, van Engelshoven JM, de Leeuw PW, Kroon AA. Vascular calcifications as a marker of increased cardiovascular risk: a meta-analysis. Vascular health and risk management. 2009;5(1):185-97.

12.   Shaw LJ, Giambrone AE, Blaha MJ, Knapper JT, Berman DS, Bellam N, Quyyumi A, Budoff MJ, Callister TQ, Min JK. Long-Term Prognosis After Coronary Artery Calcification Testing in Asymptomatic Patients: A Cohort Study. Annals of internal medicine. 2015;163(1):14-21.

13.   Wasilewski GB, Vervloet MG, Schurgers LJ. The Bone-Vasculature Axis: Calcium Supplementation and the Role of Vitamin K. Frontiers in cardiovascular medicine. 2019;6:6.

14.   Jovanovich A, Kendrick J. Personalized Management of Bone and Mineral Disorders and Precision Medicine in End-Stage Kidney Disease. Seminars in nephrology. 2018;38(4):397-409.

15.   Kim JK, Moon SJ, Park HC, Lee JS, Sim SR, Bae SC, Ha SK. Effects of lowering dialysate calcium concentrations on arterial stiffness in patients undergoing hemodialysis. The Korean journal of internal medicine. 2011;26(3):320-7.

16.   Lei Y, Nosoudi N, Vyavahare N. Targeted chelation therapy with EDTA-loaded albumin nanoparticles regresses arterial calcification without causing systemic side effects. Journal of controlled release: official journal of the Controlled Release Society. 2014;196:79-86.

17.   Tölle M, Reshetnik A, Schuchardt M, Höhne M, van der Giet M. Arteriosclerosis and vascular calcification: causes, clinical assessment and therapy. European journal of clinical investigation. 2015;45(9):976-85.

18.   Wu M, Rementer C, Giachelli CM. Vascular calcification: an update on mechanisms and challenges in treatment. Calcified tissue international. 2013;93(4):365-73.

19.   Bian S, Guo H, Ye P, Luo L, Wu H, Xiao W. Serum uric Acid level and diverse impacts on regional arterial stiffness and wave reflection. Iranian journal of public health. 2012;41(8):33-41.

20.   Chen W, Melamed ML. Vascular calcification in predialysis CKD: common and deadly. Clinical journal of the American Society of Nephrology: CJASN. 2015;10(4):551-3.

21.   Nelson AJ, Raggi P, Wolf M, Gold AM, Chertow GM, Roe MT. Targeting Vascular Calcification in Chronic Kidney Disease. JACC Basic to translational science. 2020;5(4):398-412.

22.   O'Neill WC, Lomashvili KA. Recent progress in the treatment of vascular calcification. Kidney international. 2010;78(12):1232-9.

23.   Sekikawa A, Shin C, Curb JD, Barinas-Mitchell E, Masaki K, El-Saed A, Seto TB, Mackey RH, Choo J, Fujiyoshi A, Miura K, Edmundowicz D, Kuller LH, Ueshima H, Sutton-Tyrrell K. Aortic stiffness and calcification in men in a population-based international study. Atherosclerosis. 2012;222(2):473-7.

24.   Kendrick J, Kestenbaum B, Chonchol M. Phosphate and cardiovascular disease. Advances in chronic kidney disease. 2011;18(2):113-9.

25.   Lee SJ, Lee IK, Jeon JH. Vascular Calcification-New Insights Into Its Mechanism. International journal of molecular sciences. 2020;21(8).

26.   Zhu Y, Ma WQ, Han XQ, Wang Y, Wang X, Liu NF. Advanced glycation end products accelerate calcification in VSMCs through HIF-1α/PDK4 activation and suppress glucose metabolism. Scientific reports. 2018;8(1):13730.

27.   Hénaut L, Chillon JM, Kamel S, Massy ZA. Updates on the Mechanisms and the Care of Cardiovascular Calcification in Chronic Kidney Disease. Seminars in nephrology. 2018;38(3):233-50.

28.   Hortells L, Sosa C, Guillén N, Lucea S, Millán Á, Sorribas V. Identifying early pathogenic events during vascular calcification in uremic rats. Kidney international. 2017;92(6):1384-94.

29.   Li Y, Sun Z, Zhang L, Yan J, Shao C, Jing L, Li L, Wang Z. Role of Macrophages in the Progression and Regression of Vascular Calcification. Frontiers in pharmacology. 2020;11:661.

30.   Doherty TM, Asotra K, Fitzpatrick LA, Qiao JH, Wilkin DJ, Detrano RC, Dunstan CR, Shah PK, Rajavashisth TB. Calcification in atherosclerosis: bone biology and chronic

inflammation at the arterial crossroads. Proceedings of the National Academy of Sciences of the United States of America. 2003;100(20):11201-6.

31.   Kakani E, Elyamny M, Ayach T, El-Husseini A. Pathogenesis and management of vascular calcification in CKD and dialysis patients. Seminars in dialysis. 2019;32(6):553-61.

32.   Giachelli CM. Vascular calcification mechanisms. Journal of the American Society of Nephrology : JASN. 2004;15(12):2959-64.

33.   Lanzer P, Boehm M, Sorribas V, Thiriet M, Janzen J, Zeller T, St Hilaire C, Shanahan C. Medial vascular calcification revisited: review and perspectives. European heart journal. 2014;35(23):1515-25.

34.   Zazzeroni L, Faggioli G, Pasquinelli G. Mechanisms of Arterial Calcification: The Role of Matrix Vesicles. European journal of vascular and endovascular surgery: the official journal of the European Society for Vascular Surgery. 2018;55(3):425-32.

35.   Mizobuchi M, Towler D, Slatopolsky E. Vascular calcification: the killer of patients with chronic kidney disease. Journal of the American Society of Nephrology: JASN. 2009;20(7):1453-64.

36.   Sharaf El Din UA, Salem MM, Abdulazim DO. Vascular calcification: When should we interfere in chronic kidney disease patients and how? World journal of nephrology. 2016;5(5):398-417.

37.   Vervloet M, Cozzolino M. Vascular calcification in chronic kidney disease: different bricks in the wall? Kidney international. 2017;91(4):808-17.

38.   Paloian NJ, Giachelli CM. A current understanding of vascular calcification in CKD. American journal of physiology Renal physiology. 2014;307(8):F891-900.

39.   Ciceri P, Elli F, Cappelletti L, Tosi D, Braidotti P, Bulfamante G, Cozzolino M. A new in vitro model to delay high phosphate-induced vascular calcification progression. Molecular and cellular biochemistry. 2015;410(1-2):197-206.

40.   Frismantiene A, Philippova M, Erne P, Resink TJ. Smooth muscle cell-driven vascular diseases and molecular mechanisms of VSMC plasticity. Cellular signalling. 2018;52:48-64.

41.   Shanahan CM, Crouthamel MH, Kapustin A, Giachelli CM. Arterial calcification in chronic kidney disease: key roles for calcium and phosphate. Circulation research. 2011;109(6):697-711.

42.   Frauscher B, Kirsch AH, Schabhüttl C, Schweighofer K, Kétszeri M, Pollheimer M, Dragun D, Schröder K, Rosenkranz AR, Eller K, Eller P. Autophagy Protects From Uremic Vascular Media Calcification. Frontiers in immunology. 2018;9:1866.

43.   Phadwal K, Feng D, Zhu D, MacRae VE. Autophagy as a novel therapeutic target in vascular calcification. Pharmacology & therapeutics. 2020;206:107430.

44.   Dai XY, Zhao MM, Cai Y, Guan QC, Zhao Y, Guan Y, Kong W, Zhu WG, Xu MJ, Wang X. Phosphate-induced autophagy counteracts vascular calcification by reducing matrix vesicle release. Kidney international. 2013;83(6):1042-51.

45.   Olapoju SO, Adejobi OI, Le Thi X. Fibroblast growth factor 21; review on its participation in vascular calcification pathology. Vascular pharmacology. 2020;125-126:106636.

46.   Hénaut L, Mary A, Chillon JM, Kamel S, Massy ZA. The Impact of Uremic Toxins on Vascular Smooth Muscle Cell Function. Toxins. 2018;10(6).

47.   Przybylska D, Janiszewska D, Goździk A, Bielak-Zmijewska A, Sunderland P, Sikora E, Mosieniak G. NOX4 downregulation leads to senescence of human vascular smooth muscle cells. Oncotarget. 2016;7(41):66429-43.

48.   Rovillain E, Mansfield L, Caetano C, Alvarez-Fernandez M, Caballero OL, Medema RH, Hummerich H, Jat PS. Activation of nuclear factor-kappa B signalling promotes cellular senescence. Oncogene. 2011;30(20):2356-66.

49.   Wang M, Jiang L, Monticone RE, Lakatta EG. Proinflammation: the key to arterial aging. Trends in endocrinology and metabolism: TEM. 2014;25(2):72-9.

50.   Herbert KE, Mistry Y, Hastings R, Poolman T, Niklason L, Williams B. Angiotensin II-mediated oxidative DNA damage accelerates cellular senescence in cultured human vascular smooth muscle cells via telomere-dependent and independent pathways. Circulation research. 2008;102(2):201-8.

51.   Muteliefu G, Shimizu H, Enomoto A, Nishijima F, Takahashi M, Niwa T. Indoxyl sulfate promotes vascular smooth muscle cell senescence with upregulation of p53, p21, and prelamin A through oxidative stress. American journal of physiology Cell physiology. 2012;303(2):C126-34.

52.   Nakano-Kurimoto R, Ikeda K, Uraoka M, Nakagawa Y, Yutaka K, Koide M, Takahashi T, Matoba S, Yamada H, Okigaki M, Matsubara H. Replicative senescence of vascular smooth muscle cells enhances the calcification through initiating the osteoblastic transition. American journal of physiology Heart and circulatory physiology. 2009;297(5):H1673-84.

53.   Bartoli-Leonard F, Wilkinson FL, Schiro A, Inglott FS, Alexander MY, Weston R. Suppression of SIRT1 in Diabetic Conditions Induces Osteogenic Differentiation of Human Vascular Smooth Muscle Cells via RUNX2 Signalling. Scientific reports. 2019;9(1):878.

54.   Laberge RM, Awad P, Campisi J, Desprez PY. Epithelial-mesenchymal transition induced by senescent fibroblasts. Cancer microenvironment: official journal of the International Cancer Microenvironment Society. 2012;5(1):39-44.

55.   Yu H, Yue X, Zhao Y, Li X, Wu L, Zhang C, Liu Z, Lin K, Xu-Monette ZY, Young KH, Liu J, Shen Z, Feng Z, Hu W. LIF negatively regulates tumour-suppressor p53 through Stat3/ID1/MDM2 in colorectal cancers. Nature communications. 2014;5:5218.

56.   Sanchis P, Ho CY, Liu Y, Beltran LE, Ahmad S, Jacob AP, Furmanik M, Laycock J, Long DA, Shroff R, Shanahan CM. Arterial "inflammaging" drives vascular calcification in children on dialysis. Kidney international. 2019;95(4):958-72.

57.   Zingoni A, Vulpis E, Loconte L, Santoni A. NKG2D Ligand Shedding in Response to Stress: Role of ADAM10. Frontiers in immunology. 2020;11:447.

58.   Scoumanne A, Cho SJ, Zhang J, Chen X. The cyclin-dependent kinase inhibitor p21 is regulated by RNA-binding protein PCBP4 via mRNA stability. Nucleic acids research. 2011;39(1):213-24.

59.   Wong P, Iwasaki M, Somervaille TC, Ficara F, Carico C, Arnold C, Chen CZ, Cleary ML. The miR-17-92 microRNA polycistron regulates MLL leukemia stem cell potential by modulating p21 expression. Cancer research. 2010;70(9):3833-42.

60.   Sukumaran S, Xue B, Jusko WJ, Dubois DC, Almon RR. Circadian variations in gene expression in rat abdominal adipose tissue and relationship to physiology. Physiological genomics. 2010;42a(2):141-52.

61.   Liu G, Hao P, Xu J, Wang L, Wang Y, Han R, Ying M, Sui S, Liu J, Li X. Upregulation of microRNA-17-5p contributes to hypoxia-induced proliferation in human

pulmonary artery smooth muscle cells through modulation of p21 and PTEN. Respiratory research. 2018;19(1):200.

62.   Nakanishi A, Minami A, Kitagishi Y, Ogura Y, Matsuda S. BRCA1 and p53 tumor suppressor molecules in Alzheimer's disease. International journal of molecular sciences. 2015;16(2):2879-92.

63.   Zhang X, Liu D, Hayashida Y, Okazoe H, Hashimoto T, Ueda N, Sugimoto M, Kakehi Y. G Protein-Coupled Receptor 87 (GPR87) Promotes Cell Proliferation in Human Bladder Cancer Cells. International journal of molecular sciences. 2015;16(10):24319-31.

64.   Zeng J, Zhang H, Liu Y, Sun W, Yi D, Zhu L, Zhang Y, Pan X, Chen Y, Zhou Y, Bian G, Lai M, Zhou Q, Liu J, Chen B, Ma F. Overexpression of p21 Has Inhibitory Effect on Human Hematopoiesis by Blocking Generation of CD43 + Cells via Cell-Cycle Regulation. International journal of stem cells. 2020;13(2):202-11.

65.   Arjunan KP, Sharma VK, Ptasinska S. Effects of atmospheric pressure plasmas on isolated and cellular DNA-a review. International journal of molecular sciences. 2015;16(2):2971-3016.

66.   Boudreau HE, Casterline BW, Burke DJ, Leto TL. Wild-type and mutant p53 differentially regulate NADPH oxidase 4 in TGF-β-mediated migration of human lung and breast epithelial cells. British journal of cancer. 2014;110(10):2569-82.

67.   Intihar TA, Martinez EA, Gomez-Pastor R. Mitochondrial Dysfunction in Huntington's Disease; Interplay Between HSF1, p53 and PGC-1α Transcription Factors. Frontiers in cellular neuroscience. 2019;13:103.

68.   Waga S, Stillman B. Cyclin-dependent kinase inhibitor p21 modulates the DNA primer-template recognition complex. Molecular and cellular biology. 1998;18(7):4177-87.

69.   Macip S, Igarashi M, Fang L, Chen A, Pan ZQ, Lee SW, Aaronson SA. Inhibition of p21-mediated ROS accumulation can rescue p21-induced senescence. The EMBO journal. 2002;21(9):2180-8.

70.   Herrmann J, Babic M, Tölle M, van der Giet M, Schuchardt M. Research Models for Studying Vascular Calcification. International journal of molecular sciences. 2020;21(6).

71.   Shin V, Zebboudj AF, Boström K. Endothelial cells modulate osteogenesis in calcifying vascular cells. Journal of vascular research. 2004;41(2):193-201.

72.   Fadini GP, Albiero M, Menegazzo L, Boscaro E, Vigili de Kreutzenberg S, Agostini C, Cabrelle A, Binotto G, Rattazzi M, Bertacco E, Bertorelle R, Biasini L, Mion M, Plebani M, Ceolotto G, Angelini A, Castellani C, Menegolo M, Grego F, Dimmeler S, Seeger F, Zeiher A, Tiengo A, Avogaro A. Widespread increase in myeloid calcifying cells contributes to ectopic vascular calcification in type 2 diabetes. Circulation research. 2011;108(9):1112-21.

73.   Eghbali-Fatourechi GZ, Lamsam J, Fraser D, Nagel D, Riggs BL, Khosla S. Circulating osteoblast-lineage cells in humans. The New England journal of medicine. 2005;352(19):1959-66.

74.   Wu M, Zhang JD, Tang RN, Crowley SD, Liu H, Lv LL, Ma KL, Liu BC. Elevated PTH induces endothelial-to-chondrogenic transition in aortic endothelial cells. American journal of physiology Renal physiology. 2017;312(3):F436-f44.

75.   Prüfer J, Schuchardt M, Tölle M, Prüfer N, Höhne M, Zidek W, van der Giet M. Harmful effects of the azathioprine metabolite 6-mercaptopurine in vascular cells: induction of mineralization. PloS one. 2014;9(7):e101709.

76.   Li Q, Sundberg JP, Levine MA, Terry SF, Uitto J. The effects of bisphosphonates on ectopic soft tissue mineralization caused by mutations in the ABCC6 gene. Cell cycle (Georgetown, Tex). 2015;14(7):1082-9.

77.   Schuchardt M, Tölle M, Prüfer J, Prüfer N, Huang T, Jankowski V, Jankowski J, Zidek W, van der Giet M. Uridine adenosine tetraphosphate activation of the purinergic receptor P2Y enhances in vitro vascular calcification. Kidney international. 2012;81(3):256-65.

78.   Vo TM, Disthabanchong S. Are there ways to attenuate arterial calcification and improve cardiovascular outcomes in chronic kidney disease? World journal of cardiology. 2014;6(5):216-26.

79.   Zhang X, Li R, Qin X, Wang L, Xiao J, Song Y, Sheng X, Guo M, Ji X. Sp1 Plays an Important Role in Vascular Calcification Both In Vivo and In Vitro. Journal of the American Heart Association. 2018;7(6).

80.   Akiyoshi T, Ota H, Iijima K, Son BK, Kahyo T, Setou M, Ogawa S, Ouchi Y, Akishita M. A novel organ culture model of aorta for vascular calcification. Atherosclerosis. 2016;244:51-8.

81.   Smith BJ. SDS Polyacrylamide Gel Electrophoresis of Proteins. Methods in molecular biology (Clifton, NJ). 1984;1:41-55.

82.   Studier FW. Slab-gel electrophoresis. Trends in biochemical sciences. 2000;25(12):588-90.

83.   Somer L, Shmulman O, Dror T, Hashmueli S, Kashi Y. The eukaryote chaperonin CCT is a cold shock protein in Saccharomyces cerevisiae. Cell stress & chaperones. 2002;7(1):47-54.

84.   Ghosh R, Gilda JE, Gomes AV. The necessity of and strategies for improving confidence in the accuracy of western blots. Expert review of proteomics. 2014;11(5):549-60.

85.   Sun A, Zou Y, Wang P, Xu D, Gong H, Wang S, Qin Y, Zhang P, Chen Y, Harada M, Isse T, Kawamoto T, Fan H, Yang P, Akazawa H, Nagai T, Takano H, Ping P, Komuro I, Ge J. Mitochondrial aldehyde dehydrogenase 2 plays protective roles in heart failure after myocardial infarction via suppression of the cytosolic JNK/p53 pathway in mice. Journal of the American Heart Association. 2014;3(5):e000779.

86.   Herrmann J, Xia M, Gummi MR, Greco A, Schacke A, van der Giet M, Tölle M, Schuchardt M. Stressor-Induced "Inflammaging" of Vascular Smooth Muscle Cells via Nlrp3-Mediated Pro-inflammatory Auto-Loop. Frontiers in cardiovascular medicine. 2021;8(1932):752305.

87.   Schuchardt M, Siegel NV, Babic M, Reshetnik A, Lützenberg R, Zidek W, van der Giet M, Tölle M. A Novel Long-Term ex vivo Model for Studying Vascular Calcification Pathogenesis: The Rat Isolated-Perfused Aorta. Journal of vascular research. 2020;57(1):46-52.

88.   Li L, Dai HJ, Ye M, Wang SL, Xiao XJ, Zheng J, Chen HY, Luo YH, Liu J. Lycorine induces cell-cycle arrest in the G0/G1 phase in K562 cells via HDAC inhibition. Cancer cell international. 2012;12(1):49.

89.   Duechting A, Tschöpe C, Kaiser H, Lamkemeyer T, Tanaka N, Aberle S, Lang F, Torresi J, Kandolf R, Bock CT. Human parvovirus B19 NS1 protein modulates inflammatory signaling by activation of STAT3/PIAS3 in human endothelial cells. Journal of virology. 2008;82(16):7942-52.

90.   Zhang MZ, Yao B, Cheng HF, Wang SW, Inagami T, Harris RC. Renal cortical cyclooxygenase 2 expression is differentially regulated by angiotensin II AT(1) and AT(2)

receptors. Proceedings of the National Academy of Sciences of the United States of America. 2006;103(43):16045-50.

91.   Agoglia AE, Holstein SE, Small AT, Spanos M, Burrus BM, Hodge CW. Comparison of the adolescent and adult mouse prefrontal cortex proteome. PloS one. 2017;12(6):e0178391.

92.   Taylor SC, Posch A. The design of a quantitative western blot experiment. BioMed research international. 2014;2014:361590.

93.   Gürtler A, Kunz N, Gomolka M, Hornhardt S, Friedl AA, McDonald K, Kohn JE, Posch A. Stain-Free technology as a normalization tool in Western blot analysis. Analytical biochemistry. 2013;433(2):105-11.

94.   Cabrera R, Sha Z, Vadakkan TJ, Otero J, Kriegenburg F, Hartmann-Petersen R, Dickinson ME, Chang EC. Proteasome nuclear import mediated by Arc3 can influence efficient DNA damage repair and mitosis in Schizosaccharomyces pombe. Molecular biology of the cell. 2010;21(18):3125-36.

95.   Millar SA, John SG, McIntyre CW, Ralevic V, Anderson SI, O'Sullivan SE. An Investigation Into the Role of Osteocalcin in Human Arterial Smooth Muscle Cell Calcification. Frontiers in endocrinology. 2020;11:369.

96.   Gilda JE, Gomes AV. Stain-Free total protein staining is a superior loading control to β-actin for Western blots. Analytical biochemistry. 2013;440(2):186-8.

97.   Herrmann J, Gummi MR, Xia M, van der Giet M, Tölle M, Schuchardt M. Vascular Calcification in Rodent Models-Keeping Track with an Extented Method Assortment. Biology. 2021;10(6).

98.   Russell W.M.S. BRL. The Principles of Humane Experimental Technique. London UK: Methuen & Co Ltd.; 1959.

99.   van Deursen JM. The role of senescent cells in ageing. Nature. 2014;509(7501):439-46.

100.   Campisi J, Robert L. Cell senescence: role in aging and age-related diseases. Interdisciplinary topics in gerontology. 2014;39:45-61.

101.   Kumari R, Jat P. Mechanisms of Cellular Senescence: Cell Cycle Arrest and Senescence Associated Secretory Phenotype. Frontiers in cell and developmental biology. 2021;9:645593.

102.   Childs BG, Durik M, Baker DJ, van Deursen JM. Cellular senescence in aging and age-related disease: from mechanisms to therapy. Nature medicine. 2015;21(12):1424-35.

103.   Noureddine H, Gary-Bobo G, Alifano M, Marcos E, Saker M, Vienney N, Amsellem V, Maitre B, Chaouat A, Chouaid C, Dubois-Rande JL, Damotte D, Adnot S. Pulmonary artery smooth muscle cell senescence is a pathogenic mechanism for pulmonary hypertension in chronic lung disease. Circulation research. 2011;109(5):543-53.

104.   Grootaert MOJ, Moulis M, Roth L, Martinet W, Vindis C, Bennett MR, De Meyer GRY. Vascular smooth muscle cell death, autophagy and senescence in atherosclerosis. Cardiovascular research. 2018;114(4):622-34.

105.   Nagahama K, Utsumi T, Kumano T, Maekawa S, Oyama N, Kawakami J. Discovery of a new function of curcumin which enhances its anticancer therapeutic potency. Scientific reports. 2016;6:30962.

106.   Fernandes RS, Silva JO, Mussi SV, Lopes SCA, Leite EA, Cassali GD, Cardoso VN, Townsend DM, Colletti PM, Ferreira LAM, Rubello D, de Barros ALB. Nanostructured Lipid Carrier Co-loaded with Doxorubicin and Docosahexaenoic Acid as a Theranostic Agent: Evaluation of Biodistribution and Antitumor Activity in Experimental Model. Molecular imaging and biology. 2018;20(3):437-47.

107.   Dechwongya P, Limpisood S, Boonnak N, Mangmool S, Takeda-Morishita M, Kulsirirat T, Rukthong P, Sathirakul K. The Intestinal Efflux Transporter Inhibition Activity of Xanthones from Mangosteen Pericarp: An In Silico, In Vitro and Ex Vivo Approach. Molecules (Basel, Switzerland). 2020;25(24).

108.   Hou JG, Jeon BM, Yun YJ, Cui CH, Kim SC. Ginsenoside Rh2 Ameliorates Doxorubicin-Induced Senescence Bystander Effect in Breast Carcinoma Cell MDA-MB-231 and Normal Epithelial Cell MCF-10A. International journal of molecular sciences. 2019;20(5).

109.   Chi C, Li DJ, Jiang YJ, Tong J, Fu H, Wu YH, Shen FM. Vascular smooth muscle cell senescence and age-related diseases: State of the art. Biochimica et biophysica acta Molecular basis of disease. 2019;1865(7):1810-21.

110.   Kusaczuk M, Krętowski R, Bartoszewicz M, Cechowska-Pasko M. Phenylbutyrate-a pan-HDAC inhibitor-suppresses proliferation of glioblastoma LN-229 cell line. Tumour biology: the journal of the International Society for Oncodevelopmental Biology and Medicine. 2016;37(1):931-42.

111.   Fleck O, Fahnøe U, Løvschal KV, Gasasira MU, Marinova IN, Kragelund BB, Carr AM, Hartsuiker E, Holmberg C, Nielsen O. Deoxynucleoside Salvage in Fission Yeast Allows Rescue of Ribonucleotide Reductase Deficiency but Not Spd1-Mediated Inhibition of Replication. Genes. 2017;8(5).

112.   Kramer HB, Lai CF, Patel H, Periyasamy M, Lin ML, Feller SM, Fuller-Pace FV, Meek DW, Ali S, Buluwela L. LRH-1 drives colon cancer cell growth by repressing the expression of the CDKN1A gene in a p53-dependent manner. Nucleic acids research. 2016;44(2):582-94.

113.   Kawata S, Ariumi Y, Shimotohno K. p21(Waf1/Cip1/Sdi1) prevents apoptosis as well as stimulates growth in cells transformed or immortalized by human T-cell leukemia virus type 1-encoded tax. Journal of virology. 2003;77(13):7291-9.

114.   Landskron G, De la Fuente M, Thuwajit P, Thuwajit C, Hermoso MA. Chronic inflammation and cytokines in the tumor microenvironment. Journal of immunology research. 2014;2014:149185.

115.   Orlando S, Gallastegui E, Besson A, Abril G, Aligué R, Pujol MJ, Bachs O. p27Kip1 and p21Cip1 collaborate in the regulation of transcription by recruiting cyclin-Cdk complexes on the promoters of target genes. Nucleic acids research. 2015;43(14):6860-73.

116.   Nakano M, Nakashima A, Nagano T, Ishikawa S, Kikkawa U, Kamada S. Branched-chain amino acids enhance premature senescence through mammalian target of rapamycin complex I-mediated upregulation of p21 protein. PloS one. 2013;8(11):e80411.

117.   Li S, Zhan JK, Wang YJ, Lin X, Zhong JY, Wang Y, Tan P, He JY, Cui XJ, Chen YY, Huang W, Liu YS. Exosomes from hyperglycemia-stimulated vascular endothelial

cells contain versican that regulate calcification/senescence in vascular smooth muscle cells. Cell & bioscience. 2019;9:1.

118.   Wortmann M, Arshad M, Hakimi M, Böckler D, Dihlmann S. Deficiency in Aim2 affects viability and calcification of vascular smooth muscle cells from murine aortas and angiotensin-II induced aortic aneurysms. Molecular medicine (Cambridge, Mass). 2020;26(1):87.

119.   Mijit M, Caracciolo V, Melillo A, Amicarelli F, Giordano A. Role of p53 in the Regulation of Cellular Senescence. Biomolecules. 2020;10(3).

120.   Qian Y, Chen X. Senescence regulation by the p53 protein family. Methods in molecular biology (Clifton, NJ). 2013;965:37-61.

121.   Maiuthed A, Ninsontia C, Erlenbach-Wuensch K, Ndreshkjana B, Muenzner JK, Caliskan A, Husayn AP, Chaotham C, Hartmann A, Vial Roehe A, Mahadevan V, Chanvorachote P, Schneider-Stock R. Cytoplasmic p21 Mediates 5-Fluorouracil Resistance by Inhibiting Pro-Apoptotic Chk2. Cancers. 2018;10(10).

122.   Gayrard N, Muyor K, Notarnicola C, Duranton F, Jover B, Argilés À. Optimisation of cell and ex vivo culture conditions to study vascular calcification. PloS one. 2020;15(3):e0230201.

123.   Vervloet MG, van Ballegooijen AJ. Prevention and treatment of hyperphosphatemia in chronic kidney disease. Kidney international. 2018;93(5):1060-72.

124.   Iijima K. [Hyperphosphatemia and cardiovascular diseases: impact of vascular calcification and endothelial dysfunction]. Clinical calcium. 2012;22(10):1505-13.

125.   Shioi A, Nishizawa Y. [Roles of hyperphosphatemia in vascular calcification]. Clinical calcium. 2009;19(2):180-5.

126.   Holmar J, Noels H, Böhm M, Bhargava S, Jankowski J, Orth-Alampour S. Development, establishment and validation of in vitro and ex vivo assays of vascular calcification. Biochemical and biophysical research communications. 2020;530(2):462-70.

127.   Yang M, Fang J, Liu Q, Wang Y, Zhang Z. Role of ROS-TRPM7-ERK1/2 axis in high concentration glucose-mediated proliferation and phenotype switching of rat aortic vascular smooth muscle cells. Biochemical and biophysical research communications. 2017;494(3-4):526-33.

128. Fan X, Wu J, Yang H, Yan L, Wang S. Paeoniflorin blocks the proliferation of vascular smooth muscle cells induced by platelet‑derived growth factor‑BB through ROS mediated ERK1/2 and p38 signaling pathways. Molecular medicine reports. 2018;17(1):1676-82.

129. Kefaloyianni E, Gaitanaki C, Beis I. ERK1/2 and p38-MAPK signalling pathways, through MSK1, are involved in NF-kappaB transactivation during oxidative stress in skeletal myoblasts. Cellular signalling. 2006;18(12):2238-51.

130. Wang Z, Liu B, Zhu J, Wang D, Wang Y. Nicotine-mediated autophagy of vascular smooth muscle cell accelerates atherosclerosis via nAChRs/ROS/NF-κB signaling pathway. Atherosclerosis. 2019;284:1-10.

131. You W, Hong Y, He H, Huang X, Tao W, Liang X, Zhang Y, Li X. TGF-β mediates aortic smooth muscle cell senescence in Marfan syndrome. Aging. 2019;11(11):3574-84.

132. Zhu H, Wang Z, Dong Z, Wang C, Cao Q, Fan F, Zhao J, Liu X, Yuan M, Sun X, Peng X, Zou Y, Zhou J, Ge J, Zhou X, Zhang Y. Aldehyde dehydrogenase 2 deficiency promotes atherosclerotic plaque instability through accelerating mitochondrial ROS-mediated vascular smooth muscle cell senescence. Biochimica et biophysica acta Molecular basis of disease. 2019;1865(7):1782-92.

133. El Maï M, Marzullo M, de Castro IP, Ferreira MG. Opposing p53 and mTOR/AKT promote an in vivo switch from apoptosis to senescence upon telomere shortening in zebrafish. eLife. 2020;9.

134. Duer M, Cobb AM, Shanahan CM. DNA Damage Response: A Molecular Lynchpin in the Pathobiology of Arteriosclerotic Calcification. Arteriosclerosis, thrombosis, and vascular biology. 2020;40(7):e193-e202.

135. Huang W, Yang S, Shao J, Li YP. Signaling and transcriptional regulation in osteoblast commitment and differentiation. Frontiers in bioscience : a journal and virtual library. 2007;12:3068-92.

136. Ueta C, Iwamoto M, Kanatani N, Yoshida C, Liu Y, Enomoto-Iwamoto M, Ohmori T, Enomoto H, Nakata K, Takada K, Kurisu K, Komori T. Skeletal malformations caused by overexpression of Cbfa1 or its dominant negative form in chondrocytes. The Journal of cell biology. 2001;153(1):87-100.

137.   Ducy P. Cbfa1: a molecular switch in osteoblast biology. Developmental dynamics: an official publication of the American Association of Anatomists. 2000;219(4):461-71.

138.   Zainabadi K, Liu CJ, Guarente L. SIRT1 is a positive regulator of the master osteoblast transcription factor, RUNX2. PloS one. 2017;12(5):e0178520.

139.   Furmanik M, Chatrou M, van Gorp R, Akbulut A, Willems B, Schmidt H, van Eys G, Bochaton-Piallat ML, Proudfoot D, Biessen E, Hedin U, Perisic L, Mees B, Shanahan C, Reutelingsperger C, Schurgers L. Reactive Oxygen-Forming Nox5 Links Vascular Smooth Muscle Cell Phenotypic Switching and Extracellular Vesicle-Mediated Vascular Calcification. Circulation research. 2020;127(7):911-27.

140.   Voelkl J, Luong TT, Tuffaha R, Musculus K, Auer T, Lian X, Daniel C, Zickler D, Boehme B, Sacherer M, Metzler B, Kuhl D, Gollasch M, Amann K, Müller DN, Pieske B, Lang F, Alesutan I. SGK1 induces vascular smooth muscle cell calcification through NF-κB signaling. The Journal of clinical investigation. 2018;128(7):3024-40.

141.   Baglìo SR, Devescovi V, Granchi D, Baldini N. MicroRNA expression profiling of human bone marrow mesenchymal stem cells during osteogenic differentiation reveals Osterix regulation by miR-31. Gene. 2013;527(1):321-31.

142.   Voelkl J, Tuffaha R, Luong TTD, Zickler D, Masyout J, Feger M, Verheyen N, Blaschke F, Kuro OM, Tomaschitz A, Pilz S, Pasch A, Eckardt KU, Scherberich JE, Lang F, Pieske B, Alesutan I. Zinc Inhibits Phosphate-Induced Vascular Calcification through TNFAIP3-Mediated Suppression of NF-κB. Journal of the American Society of Nephrology: JASN. 2018;29(6):1636-48.

143.   Moe SM, Chen NX. Mechanisms of vascular calcification in chronic kidney disease. Journal of the American Society of Nephrology: JASN. 2008;19(2):213-6.

144.   Vimalraj S. Alkaline phosphatase: Structure, expression and its function in bone mineralization. Gene. 2020;754:144855.

145.   Lomashvili KA, Garg P, Narisawa S, Millan JL, O'Neill WC. Upregulation of alkaline phosphatase and pyrophosphate hydrolysis: potential mechanism for uremic vascular calcification. Kidney international. 2008;73(9):1024-30.

146.   Harmey D, Hessle L, Narisawa S, Johnson KA, Terkeltaub R, Millán JL. Concerted regulation of inorganic pyrophosphate and osteopontin by akp2, enpp1, and ank: an

integrated model of the pathogenesis of mineralization disorders. The American journal of pathology. 2004;164(4):1199-209.

147.   Murshed M, Harmey D, Millán JL, McKee MD, Karsenty G. Unique coexpression in osteoblasts of broadly expressed genes accounts for the spatial restriction of ECM mineralization to bone. Genes & development. 2005;19(9):1093-104.

Statutory Declaration

"I, Meng-Di Xia, by personally signing this document in lieu of an oath, hereby affirm that I prepared the submitted dissertation on the topic: **Senescence signaling pathway in the process of vascular calcification both in vitro and ex vivo / Seneszenz-Signalweg im Prozess der Gefäßverkalkung sowohl in vitro als auch ex vivo**", independently and without the support of third parties, and that I used no other sources and aids than those stated.

All parts which are based on the publications or presentations of other authors, either in letter or in spirit, are specified as such in accordance with the citing guidelines. The sections on methodology (in particular regarding practical work, laboratory regulations, statistical processing) and results (in particular regarding figures, charts and tables) are exclusively my responsibility.

Furthermore, I declare that I have correctly marked all of the data, the analyses, and the conclusions generated from data obtained in collaboration with other persons, and that I have correctly marked my own contribution and the contributions of other persons (cf. declaration of contribution). I have correctly marked all texts or parts of texts that were generated in collaboration with other persons.

My contributions to any publications to this dissertation correspond to those stated in the below joint declaration made together with the supervisor. All publications created within the scope of the dissertation comply with the guidelines of the ICMJE (International Committee of Medical Journal Editors; www.icmje.org) on authorship. In addition, I declare that I shall comply with the regulations of Charité – Universitätsmedizin Berlin on ensuring good scientific practice.

I declare that I have not yet submitted this dissertation in identical or similar form to another Faculty.

The significance of this statutory declaration and the consequences of a false statutory declaration under criminal law (Sections 156, 161 of the German Criminal Code) are known to me."

Date   Signature

Declaration of your own contribution to the publications

Meng-Di Xia contributed the following to the below listed publications:

1. Herrmann J, Gummi MR, **Xia M**, van der Giet M, Tölle M, Schuchardt M.
    Vascular Calcification in Rodent Models-Keeping Track with an Extented Method Assortment.

    Biology (Basel). 2021;10(6):459. DOI: 10.3390/biology10060459.

    - Literature preparation (in particular for part 2, 3.1, 3.2)

    - Original draft preparation (in particular for part 2, 3.1, 3.2)

    - Read and approved the final version of the manuscript

2. Herrmann J, **Xia M**, Gummi MR, Greco A, van der Giet M, Tölle M, Schuchardt M.
    Stressor-induced "inflammaging" of vascular smooth muscle cells via Nlrp3-mediated pro-inflam-

    matoryauto-loop.

    Frontiers in Cardiovascular Medicine. 2021;8(1932):752305. DOI: 10.3389/fcvm.2021.752305.

    - VSMCs isolation and stimulation

    - qPCR, RNA in situ, Western Blot analysis

    - Original draft preparation (in particular for part 2.10)

    - Results of this dissertation in Figure 9-13.

_____

Signature, date and stamp of first supervising university professor / lecturer

_____

Signature of doctoral candidate

Curriculum Vitae

My curriculum vitae does not appear in the electronic version of my paper for reasons of data protection.

Publication list

1. Herrmann J, **Xia M**, Gummi MR, Greco A, van der Giet M, Tölle M, Schuchardt M. Stressor-induced "Inflammaging" of vascular smooth muscle cells via Nlrp3-mediated pro-inflammatoryauto-loop. Front Cardiovasc Med. 2021;8(1932):752305. doi:10.3389/fcvm.2021.752305. (IF= 6.050)

2. Herrmann J, Gummi MR, **Xia M**, van der Giet M, Tölle M, Schuchardt M. Vascular Calcification in Rodent Models-Keeping Track with an Extented Method Assortment. Biology (Basel). 2021 ; 10(6):459. doi: 10.3390/biology10060459. (IF= 5.079)

3. Tölle M, Henkel C, Herrmann J, Daniel C, Babic M, **Xia M**, Schulz AM, Amann K, van der Giet M, Schuchardt M. Uremic mouse model to study vascular calcification and "inflamm-aging". J Mol Med (Berl). 2022;100(9):1321-1330. doi: 10.1007/s00109-022-02234-y. (IF= 5.606)

Acknowledgments

Learning and living in Berlin has impressed a profound meaning into my life. After two special years, we witnessed the courage and wisdom of human beings bursting out in facing diseases and challenges and allowed me to explore more profound in scientific research. Everyone I have met here has accompanied me through such a marvelous and unforgettable time.

First of all, I thank my supervisors, PD. Dr. Markus Tölle, Prof. Markus van der Giet, and Dr. Mirjam Schuchardt gave me the valuable opportunity to work in our lab and complete my project.

Additionally, I would like to thank Dr. Mirjam Schuchardt and PD. Dr. Markus Tölle again for helping me design my project and for their enthusiasm in helping me solve my difficulties. Without their warm support and sincere encouragement, I would never have achieved this promotion and enjoyed this particular moment. Dr. Mirjam Schuchardt has helped me discuss research ideas and revise my manuscript for my project many times. She has always had great research ideas, and under her guidance, I have learned the meaning of research, which will undoubtedly be of great importance for my future work. I am sure that this will continue to guide me in my future research journey and will never end.

I thank my friend, Jaqueline Herrmann, who not only helped me with my project, but we often discussed research and other life topics together. She has taught me a lot about international etiquette and culture. Her open-mindedness is my role model. She always helps me whenever I have challenges in my life or study. I believe that friendship has no distance, even when I return to China.

I thank Nana Hu and Jinwen Zhou for their help in my life and their encouragement when I was at the bottom of my experiment and life.

I thank Manasa Reddy Gummi and Anna Greco, for their help with my project. Whenever I hit a bottleneck or needed help with my project, they were always there for me, being the first to help and for bringing me an international culture and unforgettable friendships.

Confirmation by a statistician

The supporting documents from Institut für Biometrie und klinische Epidemiologie (iBikE) is attached below.

The statistical significance of the data of this project and the method of analysis were confirmed by the statistician and the following parts of the project were also improved in the way confirmed by the statistician: exploratory analysis of the data and performed using nonparametric tests; Boxplots were used to describe the results for the part of Western blot results with multiple data.

CHARITÉ

CharitéCentrum für Human- und Gesundheitswissenschaften

Charité | Campus Charité Mitte | 10117 Berlin

Institut für Biometrie und klinische Epidemiologie (iBikE)

Direktor: Prof. Dr. Geraldine Rauch

Postanschrift:
Charitéplatz 1 | 10117 Berlin
Besucheranschrift:
Reinhardtstr. 58 | 10117 Berlin

Tel. +49 (0)30 450 562171
geraldine.rauch@charite.de
https://biometrie.charite.de/

Name, Vorname: Xia, Mengdi

Emailadresse: mengdi.xia@charite.de

Matrikelnummer: 227464

PromotionsbetreuerIn: PD Dr. med. Markus Tölle

Promotionsinstitution / Klinik: Nephrologie und

internistische Intensivmedizin

Bescheinigung

Hiermit bescheinige ich, dass Mengdi Xia innerhalb der Service Unit Biometrie des Instituts für Biometrie und klinische Epidemiologie (iBikE) bei mir eine statistische Beratung zu einem Promotionsvorhaben wahrgenommen hat. Folgende Beratungstermine wurden wahrgenommen:

- Termin 1: 24.11.2021

Folgende wesentliche Ratschläge hinsichtlich einer sinnvollen Auswertung und Interpretation der Daten wurden während der Beratung erteilt:

- Hinweis auf explorativen Charakter der Datenanalyse
- Nichtparametrische Tests aufgrund kleiner Fallzahl
- Boxplots für die deskriptive grafische Darstellung

Diese Bescheinigung garantiert nicht die richtige Umsetzung der in der Beratung gemachten Vorschläge, die korrekte Durchführung der empfohlenen statistischen Verfahren und die richtige Darstellung und Interpretation der Ergebnisse. Die Verantwortung hierfür obliegt allein dem Promovierenden. Das Institut für Biometrie und klinische Epidemiologie übernimmt hierfür keine Haftung.

Datum: 15.12.2021

Name der Beraterin: Mareen Pigorsch

Mareen Pigorsch

Digital unterschrieben von
Mareen Pigorsch
Datum: 2021.12.15 15:33:01
+01'00'

CHARITÉ
UNIVERSITÄTSMEDIZIN BERLIN
Institut für Biometrie und
Klinische Epidemiologie
Campus Charité Mitte
Charitéplatz 1 | D-10117 Berlin
Sitz: Reinhardtstr. 58

Unterschrift Beraterin, Institutsstempel